



**International Journal
of Engineering &
Applied Sciences**

I
J
E
A
S

IJEAS

Volume 16, Issue 3
2024

HONORARY EDITORS

(in alphabetical order)

Prof. Atluri, S.N.- University of California, Irvine-USA
Prof. Liew, K.M.- City University of Hong Kong-HONG KONG
Prof. Lim, C.W.- City University of Hong Kong-HONG KONG
Prof. Liu, G.R.- National University of Singapore- SINGAPORE
Prof. Nath, Y.- Indian Institute of Technology, INDIA
Prof. Omurtag, M.H. -ITU
Prof. Reddy, J.N.-Texas A& M University, USA
Prof. Saka, M.P.- University of Bahrain-BAHRAIN
Prof. Shen, H.S.- Shanghai Jiao Tong University, CHINA
Prof. Xiang, Y.- University of Western Sydney-AUSTRALIA
Prof. Wang, C.M.- National University of Singapore- SINGAPORE
Prof. Wei, G.W.- Michigan State University-USA

EDITOR IN CHIEF:

Assoc. Prof. Ibrahim AYDOĞDU -Akdeniz University aydogdu@akdeniz.edu.tr

ASSOCIATE EDITORS:

Assist. Prof. Kadir MERCAN –Mehmet Akif Ersoy
University kmercan@mehmetakif.edu.tr

SECTION EDITORS:

Assoc. Prof. Metin Mutlu Aydın – Ondokuz Mayıs University
Assoc. Prof. Mustafa Arda –Trakya University
Assist. Prof. Refik Burak Taymuş- Van 100. Yıl University
Dr. Shahin Nayyeri Amiri- Old Dominion University

EDITORIAL BOARD

(The name listed below is not Alphabetical or any title scale)

- Prof. Xinwei Wang -Nanjing University of Aeronautics and Astronautics
Asst. Prof. Francesco Tornabene -University of Bologna
Asst. Prof. Nicholas Fantuzzi -University of Bologna
Assoc. Prof. Keivan Kiani - K.N. Toosi University of Technology
Asst. Prof. Michele Baccocchi -University of Bologna
Asst. Prof. Hamid M. Sedighi -Shahid Chamran University of Ahvaz
Prof. Yaghoub Tadi Beni -Shahrekord University
Prof. Raffaele Barretta -University of Naples Federico II
Prof. Meltem ASILTÜRK -Akdeniz University *meltemasilturk@akdeniz.edu.tr*
Prof. Metin AYDOĞDU -Trakya University *metina@trakya.edu.tr*
Prof. Ayşe DALOĞLU - KTU *aysed@ktu.edu.tr*
Prof. Oğuzhan HASANÇEBİ - METU *oguzhan@metu.edu.tr*
Asst. Prof. Rana MUKHERJİ - The ICFAI University
Assoc. Prof. Baki ÖZTÜRK - Hacettepe University
Assoc. Prof. Yılmaz AKSU -Akdeniz University
Assoc. Prof. Hakan ERSOY- Akdeniz University
Assoc. Prof. Mustafa Özgür YAYLI -Uludağ University
Assoc. Prof. Selim L. SANİN - Hacettepe University
Asst. Prof. Engin EMSEN -Akdeniz University
Prof. Serkan DAĞ - METU
Prof. Ekrem TÜFEKÇİ - İTÜ

ABSTRACTING & INDEXING



IJEAS provides unique DOI link to every paper published.

EDITORIAL SCOPE

The journal presents its readers with broad coverage across some branches of engineering and science of the latest development and application of new solution algorithms, artificial intelligent techniques innovative numerical methods and/or solution techniques directed at the utilization of computational methods in solid and nano-scaled mechanics.

International Journal of Engineering & Applied Sciences (IJEAS) is an Open Access Journal

International Journal of Engineering & Applied Sciences (IJEAS) publish original contributions on the following topics:

Civil Engineering: numerical modelling of structures, seismic evaluation, experimental testing, construction and management, geotechnical engineering, water resources management, groundwater modelling, coastal zone modelling, offshore structures, water processes, desalination, waste-water treatment, pavement and maintenance, transport and traffic, laser scanning, and hydrographic surveying, numerical methods in solid mechanics, nanomechanic and applications, microelectromechanical systems (MEMS), vibration problems in engineering, higher order elasticity (strain gradient, couple stress, surface elasticity, nonlocal elasticity)

Electrical Engineering: artificial and machine intelligence and robotics, automatic control, bioinformatics and biomedical engineering, communications, computer engineering and networks, systems security and data encryption, electric power engineering and drives, embedded systems, Internet of Things (IoT), microwaves and optics.

Engineering Mathematics and Physics: computational and stochastic methods, optimization, nonlinear dynamics, modelling and simulation, computer science, solid state physics and electronics, computational electromagnetics, biophysics, atomic and molecular physics, thermodynamics, geophysical fluid dynamics, wave mechanics, and solid mechanics.

Mechanical Engineering: machine design, materials science, mechanics of materials, manufacturing engineering and technology, dynamics, robotics, control, industrial engineering, ergonomics, energy, combustion, heat transfer, fluids mechanics, thermodynamics, turbo machinery, aerospace research, aerodynamics, and propulsion.

IJEAS allows readers to read, download, copy, distribute, print, search, or link to the full texts of articles.



CONTENTS

The Microstructure, Hardness, and Density Investigation of Mg Composites Reinforced with Kaolin <i>By Mikail Aslan</i>	116-122
--	----------------

Reliability Assessment of Cracked Reinforced Concrete Slab and Verification using a Full-Scale in-Situ Load Test <i>By Yisihak Gebre Tarekegn, Biruktawit Taye Tarekegn, Abrham Gebre Tarekegn, Asmerom Abay</i>	123-140
--	----------------

Deflections of Cantilever Beams Subjected to A Point Load At the Free End <i>By Alper Oğulcan Söylemez, Bekir Akgöz</i>	141-152
---	----------------

Effect of Evaporation and Condensation Temperature on Performance of Organic Rankine System Using R134a, R417A, R422D, R245fa <i>By Erkan Dikmen, Arzu Şencan Şahin</i>	153-164
---	----------------



The Microstructure, Hardness, and Density Investigation of Mg Composites Reinforced with Kaolin

Mikail Aslan

Gaziantep University, Faculty of Engineering, Department of Metallurgical and Material Science Engineering, Gaziantep, Turkey

✉: mikailsln@gmail.com, : 0000-0003-2235-5104-0000

Received: 30.04.2024, Revised: 12.06.2024, Accepted: 16.06.2024

Abstract

The demand for lightweight, high-performance aerospace and automotive components is growing, prompting interest in utilizing abundant materials like magnesium and its alloys and composites. However, pure magnesium's reactivity and mechanical weaknesses hinder its use in demanding engineering applications. To address this, magnesium is often reinforced with nanoparticles, leading to the development of magnesium matrix composites with improved mechanical properties. This paper systematically investigates the effects of kaolin on microstructure, hardness, and density for magnesium composites through the use of powder metallurgy. Results indicate that increasing kaolin content generally enhances density and hardness. These findings contribute to the understanding of kaolin-reinforced magnesium composites and their potential for improved mechanical properties in various applications.

Keywords: Kaolin, Mg composites, hardness, microstructure and density measurement

1. Introduction

There exists a growing need for lightweight and economical aerospace and automotive components showing superior performance. This increases the rising interest in leveraging naturally abundant materials. Specifically, magnesium and its alloys are contemporary lightweight materials. They find extensive applications across diverse industrial sectors, ranging from aerospace and automotive to biomedical [1]. On the other hand, pure magnesium's high reactivity and weak mechanical properties make it unsuitable for demanding engineering applications. To address this, magnesium is commonly reinforced with nanoparticles [2-6]. Researchers have concentrated their efforts on developing magnesium matrix composites with various reinforcements. These composites are designed to augment the overall performance of the material by integrating reinforcements into the magnesium matrix.

A wide array of reinforcement components, including Al_2O_3 [7], B_4C [8], SiC [9], WC [10], TiC [11], TiB_2 [12], carbon nanotubes (CNT) [13, 14], and graphene nanoplatelets (GNPs) [15], have been extensively employed in the fabrication of magnesium matrix composites. The integration of these reinforcements enhances mechanical properties such as tensile strength, hardness, and wear resistance, thereby broadening the potential applications of magnesium composites. Researchers endeavor to strike a delicate balance between desired properties and the specific requirements of diverse sectors through meticulous selection and optimization of the reinforcement elements [16-19]. Anbuechhiyan et al. [20] studied TiC reinforced magnesium nanocomposites by varying its weight percentage (3%, 6% and 9%) using powder metallurgy for marine applications. As the percentage of reinforcement rises, the compressive strength and hardness of magnesium nanocomposites increase. This enhancement occurs as a result of integrating stiffer and stronger reinforcements into the matrix alloy. Raja et al. [21]



conducted a study of mechanical and microstructural properties of graphene reinforced magnesium composite. Results showed that the incorporation of graphene nanoplatelets (GNPs) has led to slight alterations in the crystallographic texture and grain size of the magnesium alloy. Additionally, there has been a remarkable increase in tensile strength, hardness, and impact strength, Ponappa et al. [22] focused on Y_2O_3 reinforced Mg composites. Scanning electron micrographs revealed a uniform distribution of Y_2O_3 particles within the magnesium and magnesium alloy matrix. Furthermore, macro and microhardness tests demonstrated a noticeable increase in hardness corresponding to the augmented amount of Y_2O_3 reinforcement.

Kaolin can be used as reinforcing particles. For instance; Zaimi et al. [23] studied Sn-Ag-Cu reinforced with kaolin with different weight percentages. In their study, the addition of 1.0 wt.% kaolin was determined to be the optimal value for enhancing the performance of the Sn-3.0Ag-0.5Cu solder. Furthermore, the incorporation of kaolin decreases the formation area of β -Sn while simultaneously increasing the eutectic area with fine intermetallic particles. Additionally, kaolin additions lead to a reduction in the undercooling value of the Sn-3.0Ag-0.5Cu solder. Ogunrinola et al. [24] conducted another study where they successfully produced aluminum metal matrix composites reinforced with silica and kaolin through the process of stir casting. The composites reinforced with kaolin exhibit higher hardness compared to those reinforced with silica sand. This difference is attributed to the higher molecular weight of kaolin.

In this paper, the microstructure evaluation, hardness, density of kaolin reinforced mg composites were studied employing powder metallurgy routine. To the best of our knowledge, this is first time study. However, pure magnesium's reactivity and mechanical weaknesses hinder its use in demanding engineering applications. To address this, magnesium was reinforced with kaolin.

2. Materials and Methods

In the fabrication of kaolin reinforced magnesium composites, magnesium and kaolin were sourced from Nanografi, and ZAG Chemistry. 10 g of samples were weighted. 3, 5, 7 and 10 weight percentages of kaolin were chosen. Then, the powders were combined in a beaker and mixed thoroughly using a magnetic stirrer for thirty minutes. The magnetic stirrer was set to 800 rpm. After achieving a homogeneous distribution, the powder samples were cold pressed in a steel die at 98 MPa to form bulk samples.

3. Results and Discussion

To produce kaolin-reinforced Mg composites, kaolin were utilized at the weight percentages of 3%, 5%, 7% and 10%. Using the Archimedeian principle, the densities of these materials were determined. Figure 1 illustrates the measured densities of the composites at varying kaolin weight percentages. As the kaolin content increases, the densities of the composites tend to rise. This outcome is anticipated, given that the density of kaolin (2.6 g/cm^3) exceeds that of magnesium (1.738 g/cm^3). However, it's notable that the composite reinforced with 7% kaolin exhibits a lower density compared to the one reinforced with 3% kaolin. This could be attributed to agglomerations within the structure. This leads to increased internal voids, thereby compromising the composite's density. Consequently, this weakens the overall strength of the density of the composite. Similar observations have been reported in studies involving various types of reinforcement particles [14, 25, 26].

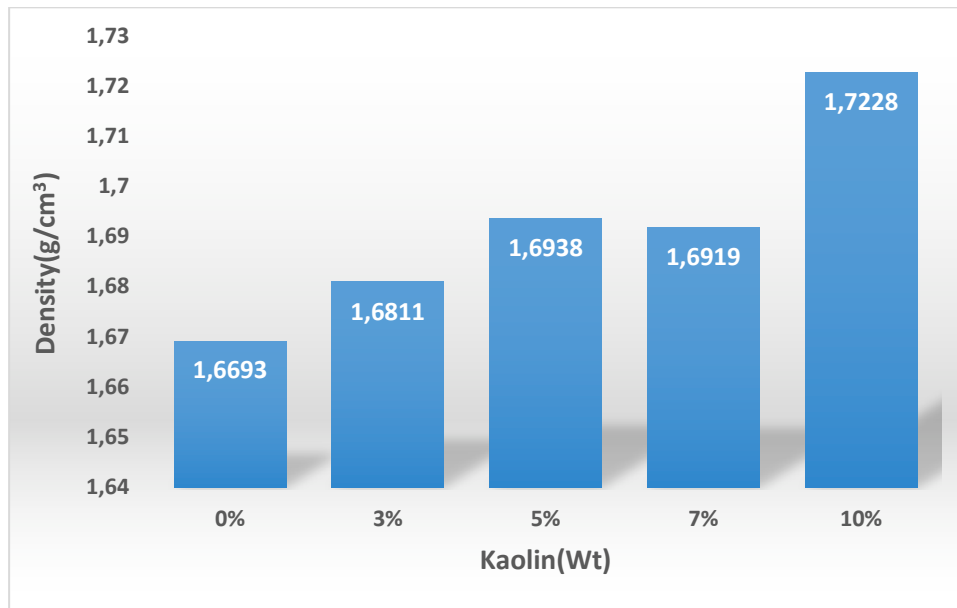


Fig. 1 The density measurements of the given kaolin weight percentages.

The metallographic procedures involving sanding and polishing were applied. Sanding was performed using 1000 and 2000 mesh sanders to refine the material surfaces. Subsequently, the specimens underwent polishing with 6 μ diamond suspension, followed by 3 μ diamond suspension to attain a polished finish of higher quality. To assess the hardness of the investigated composites, measurements were conducted using an AOB Vickers Microhardness tester with a load of 0.3 kgf and a dwell time of 10 seconds. Each sample underwent ten indentations, and the average hardness values were recorded. Fig. 2 illustrates the Vickers hardness values of the composites. The highest hardness value was observed in the composite with a 10% weight percentage of kaolin. Furthermore, an increase in the kaolin content correlates with an increase in hardness. However, there is a decrease in hardness observed at the 7% weight percentage of kaolin when compared to the other composites. These findings are consistent with density measurements.

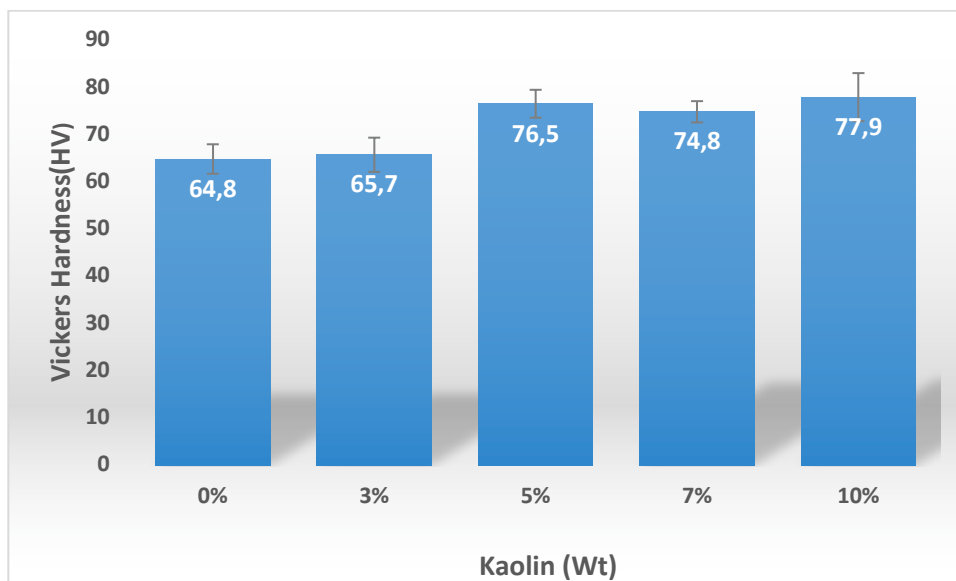


Fig. 2 The vickers hardness measurements of the given weight percentages of kaolin

Fig. 3 displays optical images of the given structures. Within these structures, metallographic spots are visible, indicative of contamination. Upon closer examination, some kaolin particles are observed at the Mg/Mg interfaces or within Mg/MgO, while others are enveloped within the Mg particles. Another notable feature is that the grain size of pure Mg is notably smaller compared to that of other composites. Additionally, MgO oxide particles are present in the structures. These dispersed oxide particles are expected to contribute to the reinforcement of the composites to some extent.

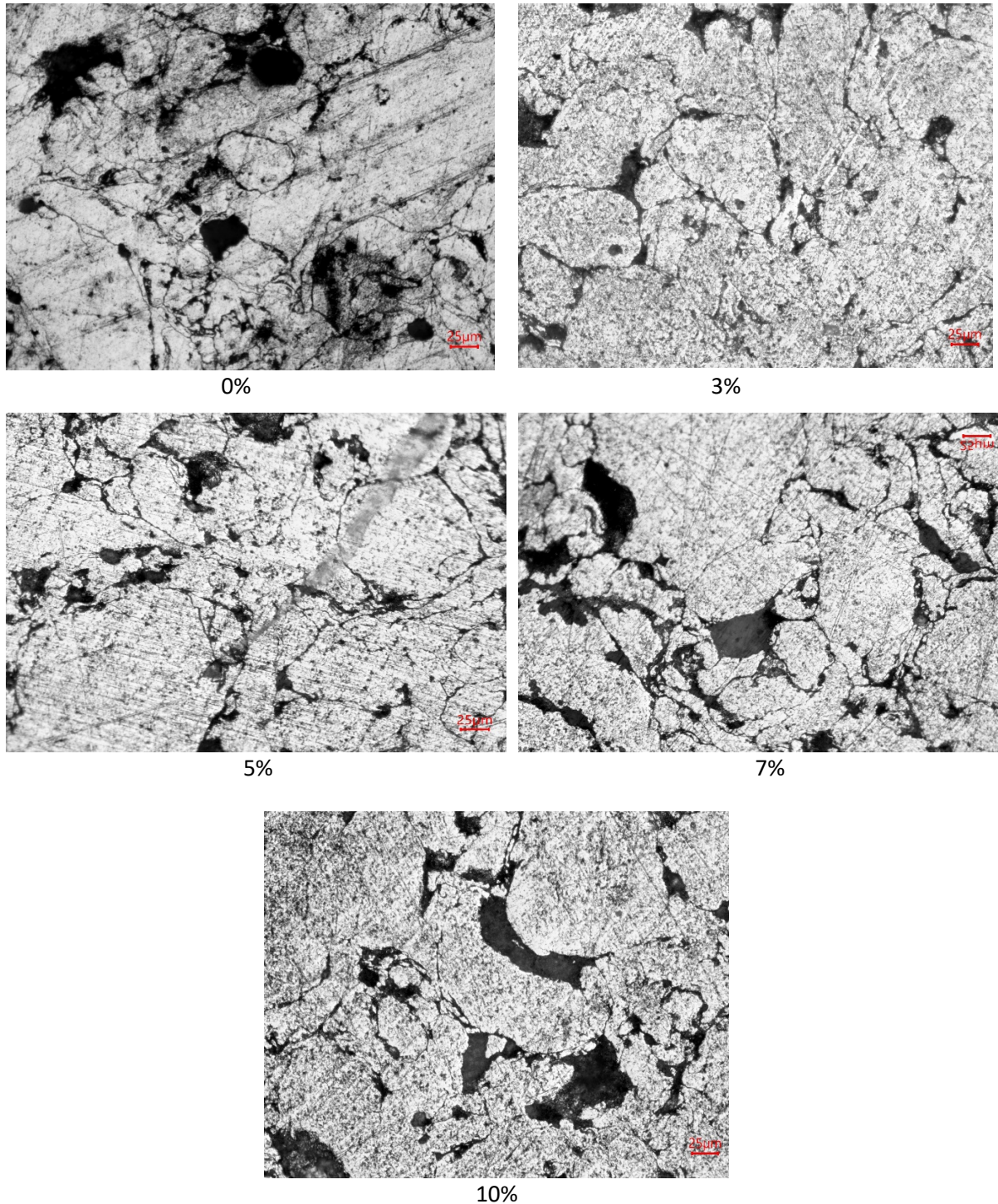


Fig. 3 Optical Image view of the given composites

4. Conclusion

This study aimed to fabricate magnesium composites reinforced with kaolin through a powder metallurgy process. Magnesium was selected as the matrix material, with kaolin serving as the reinforcing component. The main goal was to analyze how different ratios of kaolin affect the properties of the resulting metal matrix composites.

It's worth noting that the composite reinforced with 7% kaolin demonstrates a lower density in comparison to the counterpart reinforced with 3% kaolin. This phenomenon could be attributed to agglomerations within the structure, resulting in increased internal voids and consequently compromising the composite's density. As a result, this weakening effect extends to the overall strength of the composite.

The composite containing 10% kaolin by weight exhibited the highest hardness value. Additionally, there was a direct correlation between kaolin content and hardness, with an increase in kaolin concentration resulting in higher hardness values. However, a decrease in hardness was noted at the 7% kaolin weight percentage compared to the other composites. These observations align with the findings from density measurement

5. References

- [1] Tan J, Ramakrishna S. Applications of Magnesium and Its Alloys: A Review. *Applied Sciences*, 11, 6861-6881, 2021.
- [2] Zhan H, Zhang J, Miao J, Wang C, Zeng G, Wang J, et al., A low-cost Mg–Al–Mn–Zn alloy for automotive road wheel applications. *Materials Science and Engineering: A*, 897, 146321, 2024.
- [3] Seikh Z, Sekh M, Mandal G, Sengupta B, Sinha A, Metal Matrix Composites Processed Through Powder Metallurgy: A Brief Overview. *Journal of The Institution of Engineers (India)*, Series D, 1-8, 2024.
- [4] Rajan AV, Krishnan BR, Sundaram CM, Investigation and characteristics of AZ91 magnesium metal matrix composite using the powder metallurgy process. *Bulletin of the Chemical Society of Ethiopia*, 38, 305-12, 2024.
- [5] Guo R, Le Q, Wang Y, Ren L, Jiang Y, Li D, et al., Effect of ZrO₂p on the Microstructure and Mechanical Properties of the AZ31 Magnesium Alloy. *JOM*, 76, 1690-701, 2024.
- [6] Faisal N, Kumar D, Kumar A, Ansu AK, Sharma A, Jain AK, et al., Experimental Analysis for the Performance Assessment and Characteristics of Enhanced Magnesium Composites Reinforced with Nano-Sized Silicon Carbide Developed Using Powder Metallurgy. *ACS Omega*, 9, 5230-45, 2024.
- [7] Niranjana CA, Shobha R, Prabhuswamy NR, Yogesh HM, Jain VKS, Reciprocating Dry Sliding Wear Behaviour of AZ91/Al₂O₃ Magnesium Nanocomposites. *Arabian Journal for Science and Engineering*, 49, 2299-310, 2024.


- [8] Titarmare V, Banerjee S, Sahoo P, Abrasive wear behavior of AZ31–B4C composites. *Tribology International*, 194, 109455, 2024.
- [9] Li C-P, Li Y-Q, Li C-F, Chen H-Y, Ma Y-L, Effect of SiC on Microstructure and Mechanical Properties of Nano-SiC/Mg-8Al-1Sn Composites. *Journal of Materials Engineering and Performance*, 1-10, 2024.
- [10] Banerjee S, Poria S, Sutradhar G, Sahoo P, Abrasive wear behavior of WC nanoparticle reinforced magnesium metal matrix composites. *Surface Topography: Metrology and Properties*, 8, 025001, 2020.
- [11] Anasori B, Caspi EaN, Barsoum MW, Fabrication and mechanical properties of pressureless melt infiltrated magnesium alloy composites reinforced with TiC and Ti₂AlC particles. *Materials Science and Engineering: A*, 618, 511-22, 2014.
- [12] Meher A, Mahapatra MM, Samal P, Vundavilli PR, Study on effect of TiB₂ reinforcement on the microstructural and mechanical properties of magnesium RZ5 alloy based metal matrix composites. *Journal of Magnesium and Alloys*, 8, 780-92, 2020.
- [13] Say Y, Guler O, Dikici B, Carbon nanotube (CNT) reinforced magnesium matrix composites: The effect of CNT ratio on their mechanical properties and corrosion resistance. *Materials Science and Engineering: A*, 798, 139636, 2020.
- [14] Aslan M, *Mechanical and Optical Properties of Multiwall Carbon Nanotube-Reinforced ZA27-Al₂O₃ Hybrid Composites Fabricated by Powder Metallurgy Routine*. *International Journal of Engineering and Applied Sciences*, 15, 86-94, 2023.
- [15] Rashad M, Pan F, Asif M, Magnesium matrix composites reinforced with graphene nanoplatelets. *Graphene Materials: Fundamentals and Emerging Applications*, 151-89, 2015.
- [16] Akbas SD, Numanoglu HM, Akgöz B, Civalek Ö, Application of Newmark Average Acceleration and Ritz Methods on Dynamical Analysis of Composite Beams under a Moving Load. *Journal of Applied and Computational Mechanics*, 8, 764-73, 2022.
- [17] Anasori B, El'ad NC, Barsoum MWJMS, A E, Fabrication and mechanical properties of pressureless melt infiltrated magnesium alloy composites reinforced with TiC and Ti₂AlC particles. *Materials Science and Engineering: A*, 618, 511-22, 2014.
- [18] Anbuechezhiyan G, Mohan B, Kathiresan S, Pugazenthi RJMTP, Influence of microstructure and mechanical properties of TiC reinforced magnesium nano composites. *Materials Today: Proceedings*, 27, 1530-4, 2020.
- [19] Aslan Mikail, *Mechanical and Optical Properties of Multiwall Carbon Nanotube-Reinforced ZA27-Al₂O₃ Hybrid Composites Fabricated by Powder Metallurgy Routine*. *International Journal of Engineering & Applied Sciences*, 15, 86-94, 2023.

- [20] Anbuezhhiyan G, Mohan B, Kathiresan S, Pugazenthi R, Influence of microstructure and mechanical properties of TiC reinforced magnesium nano composites. *Materials Today: Proceedings*, 27, 1530-4, 2020.
- [21] Raja KSS, Kumar UM, Mathivanan S, Ganesan S, ArunKumar T, Hemanandh J, et al., Mechanical and microstructural properties of graphene reinforced magnesium composite. *Materials Today: Proceedings*, 44, 3571-4, 2021.
- [22] Ponappa K, Aravindan S, Rao PV, Influence of Y₂O₃ particles on mechanical properties of magnesium and magnesium alloy (AZ91D). *Journal of Composite Materials*, 47, 1231-9, 2013.
- [23] Zaimi NSM, Salleh MAAM, Abdullah M, Ahmad R, Mostapha M, Yoriya S, et al., Effect of kaolin geopolymer ceramic addition on the properties of Sn-3.0 Ag-0.5 Cu solder joint. *Materials Today Communications*, 25, 101469, 2020.
- [24] Ogunrinola I, Akinyemi M, Aizebeokhai A, Sule R, Sanni S, Boyo H, et al., Silica and kaolin reinforced aluminum matrix composite for heat storage. *Reviews on Advanced Materials Science*, 62, 20220305, 2023.
- [25] Aslan M, Investigation of Effect of W-Zn-Co Alloy on Microstructure And Hardness of The Epoxy Composites. *International Journal of Engineering and Applied Sciences*, 15, 144-9, 2023.
- [26] Aslan M, Eskalen H, Kavgaci M, Carbon Quantum Dot (CQD) Nanoparticles Synthesized by Sucrose and Urea: Application as Reinforcement Effect on Al–Mg–Cu–Zn Composite. *Russian Journal of General Chemistry*, 93, 2152-60, 2023.

Reliability Assessment of Cracked Reinforced Concrete Slab and Verification using a Full-Scale in-Situ Load Test

Yisihak Gebre ^{a*}, Biruktawit Taye ^b, Abrham Gebre ^c and Asmerom Weldegerima ^d

^{a, b, c, d} Addis Ababa Institute of Technology, Addis Ababa University, Ethiopia

✉: yisgeb2004@gmail.com, : 0009-0009-4127-4896 ^a, 0009-0004-6373-5132 ^b, 0000-0003-0172-2905 ^c, 0009-0000-0931-5082 ^d

Received: 15.06.2024, Revised: 16.10.2024, Accepted: 03.11.2024

Abstract

This paper presents a case study focused on the deterministic and probabilistic structural assessments of a cracked reinforced concrete (RC) slab and evaluation using in-situ load testing. The case study explores the practical application of in-situ load testing as a diagnostic tool for evaluating the condition of the slab and determining its ultimate load-carrying capacity in the presence of cracks, and service loads are used to verify its serviceability. Through comprehensive analysis and interpretation of test results, this study aims to provide valuable insights into the structural performance of cracked reinforced concrete slabs and inform effective repair and rehabilitation strategies. The building under examination is a G+4 reinforced concrete structure constructed using ready mix concrete transported to the construction site. Upon inspecting the slab, which had a total thickness of 170 mm, numerous deeply mapped cracks were evident, visible from the slab's surface and extending through its entire depth. Structural analysis indicated that the design included sufficient reinforcement and that the loads acting upon the slab were not expected to induce the cracking. Factors such as poor construction practices, potential issues with the cement used, and excessive evaporation may have contributed to the occurrence of these cracks, necessitating repairs. A full-scale in-situ load test was performed following ACI 318-08 testing procedures and results show that the slab under investigation is reasonably safe against serviceability and strength requirements with “no evidence” of failure.

Keywords: Structural assessment, RC slab, cracks, in-situ load test, load-carrying capacity

1. Introduction

Reinforced concrete slabs may develop cracks due to various factors such as loading conditions, shrinkage, temperature variations, and material deterioration. Assessing the condition of cracked RC slabs is crucial for ensuring structural safety, durability, and serviceability [1]. The occurrence of excessive evaporation from the concrete mix in the plastic stage is a factor that could lead to shrinkage in the concrete matrix. Such excessive loss of water may result in related plastic shrinkage cracks [2]. Concrete surface starts to dry on direct sun exposure and as a general rule at evaporation rates greater than 1.0 kg/m² and immediate protection/covering becomes necessary. However, drying may occur at much lesser rates of evaporation depending on the concrete mix ratio [3]. The other reason of cracks in concrete is drying shrinkage that results from the loss/evaporation of water from the concrete after hardening stage [2]. These types of cracks are known to penetrate full depths of structural members.

Cracks which affect the structural integrity of RC structures need to be treated. For such purposes, different retrofitting and/ or strengthening techniques were experimentally tested using cement grout, epoxy injection, ferrocement layer, carbon fiber strip and section enlargement. Results showed that all repair techniques are found to be able to enhance the structural capacity of cracked concrete slabs where section enlargement gives 130% higher ultimate load capacities compared to the control slab [4].



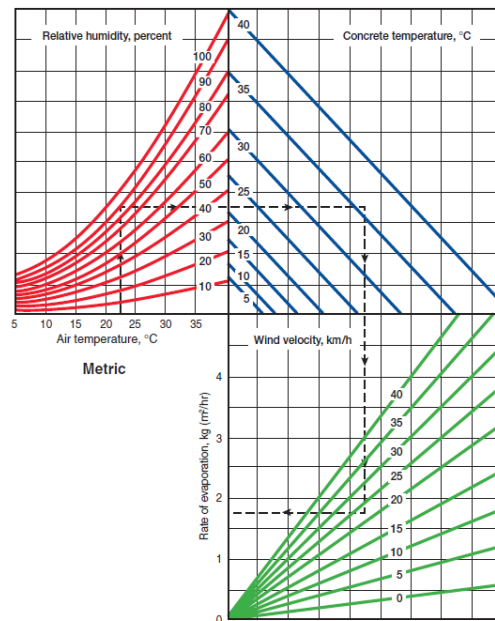


Fig. 1. Estimation of rate of evaporation [3]

Ensuring the structural integrity of existing structural slabs with limited material data and various defects, such as multiple cracks, poses a significant challenge. In-situ load testing has emerged as a valuable verification technique for addressing this challenge [5–9]. The study conducted by Saleem, Abbas, and Nehdi demonstrates that a straightforward approach involving distributed in-situ loading using cement bags, in conjunction with finite element modeling, can offer reliable insights into appraising such existing structures. These findings hold promise for assisting practitioners in effectively managing a substantial portfolio of RC slabs affected by construction defects, thereby facilitating the process of condition rating. Once the condition of cracked RC slabs is assessed, appropriate rehabilitation and strengthening strategies can be implemented to restore or enhance their structural integrity. Common repairing techniques may include crack injection, fiber reinforced polymers (FRP) strengthening, steel plate bonding, and external post-tensioning [7].

A static and dynamic analysis of an industrial hall with a reinforced concrete slab was conducted to assess the capacity of the cracked slab. The slab exhibited lots of cracks, with a maximum crack width of 1.6 mm, penetrating to depths ranging from 30 to 125 mm. The analysis results indicated that the slab's capacity remained safe, provided the service load is limited to a lower permissible limit of 4 kN/m² [6].

A five-story concrete building that was partially burned was evaluated using a non-destructive load test. According to the test results, the affected portions need retrofitting to restore the original design load carrying capacity of the as the structure's has a reduced strength [10]. Moreover, a load test was conducted on a garage structure and it was determined that the structure was adequate [11,12]. For several reasons, including determining the impact of construction and design defects and omissions, in-situ load testing is important. For the structures considered in the load test, finite-element technique models were developed to facilitate the design of the load test. The field observations were confirmed by the computational simulations [13].

In situ load testing of RC slabs in parking garage structures was performed using both cyclic and 24-hour load test approaches. Cyclic loading was applied to the structural members in a quasi-static manner over at least six loading and unloading cycles at regular intervals. Both methods produced the same result: two identical RC slabs failed to meet the acceptance criteria [11]. These findings suggest that conducting a 24-hour load test is a practical approach for in situ testing of existing RC

slabs. Similarly, in situ load tests were conducted on RC and prestressed concrete (PC) slabs, with measurements taken for deflection and crack width. The results were compared against the limits specified in ACI 318 and ACI 437 standards. The paper also presented the evaluation criteria and findings from two field projects: one involving a post-tensioned concrete slab with structural deficiencies due to tendon and mild reinforcement misplacement, and another concerning a floor bay of a two-way RC slab showing cracks in both the positive and negative moment regions. The testing revealed that, in some cases, the ACI 437 requirements were not met [8].

Several studies have attempted in situ load testing on RC slabs. Among them, W.J. Gold and A. Nanni conducted an in situ load test by varying the load magnitude, applying cyclic loads over a short period to address the lack of having accepted standardized design and construction specifications for new structural repairs. The test results demonstrated that the performance of the strengthening system using bonded carbon fiber-reinforced polymer (CFRP) sheets was found effective [14].

Different codes and standards provide the minimum magnitude of loads to be used for load test in buildings. As per the requirement of ACI 318-08, the intensity of the load to be applied to the slab is specified that the total test load including dead load already in place shall not be less than the magnitude given in Eq. (1) and the load shall be applied in not less than four approximately equal increments [15].

$$LI_{min} \geq 0.85(\gamma_D D + \gamma_L L) \quad (1)$$

where LI_{min} is the minimum load intensity (kN/m^2), D , L are dead and live load effects, respectively (kN/m^2), γ_D and γ_L are dead and live load factors, respectively.

The maximum deflection of the slab during test load shall satisfy one of the following conditions given in Eqs. (2) and (3) [15].

$$\Delta_{max} \leq \frac{L_1^2}{20,200h} \quad (2)$$

$$\Delta_{r,max} \leq \frac{\Delta_{max}}{4} \quad (3)$$

where Δ_{max} is the measured maximum deflection (mm), L_1 is the shorter span for two-way slab systems (mm), h is the overall thickness of member (mm) and $\Delta_{r,max}$ is the measured residual deflection (mm)

In this study, evaluation of an RC slab is made analytically and by in-situ load testing. After a year of construction, a field test is carried out on a RC floor slab to confirm the findings of the design review and probabilistic assessment, thereby ensuring its safety. The results show that the slab is reasonably safe against serviceability and strength requirements, even with cracks.

2. Methodology

The structure under investigation in this research comprises five floors, encompassing the ground level and four stories above it. At the time of examination, construction had progressed up to the third story. During the construction process, cracks were observed within two days in the newly cast slabs on the third story, prompting a halt in work. This pause was necessary to assess the safety and

viability of continuing construction and future occupation of the building. Decisions regarding whether the structure could support further construction and future occupation or if partial or complete demolition and reconstruction were required hinged on this evaluation.

The verification includes strength and durability aspects. This is to assess whether the deflection requirement of the slab is exceeded or not. Moreover, load carrying capacity of the slab was assessed. Deterministic and reliability-based assessment of the structure are carried out to evaluate the safety of the structure. For the load test, the most defective slab with maximum span dimensions is selected as the panel is critical (2nd floor slab between Axis 1-2 and Axis A-B). Fig. 2 presents the floor plan of the building, indicating the locations of the observed cracks.

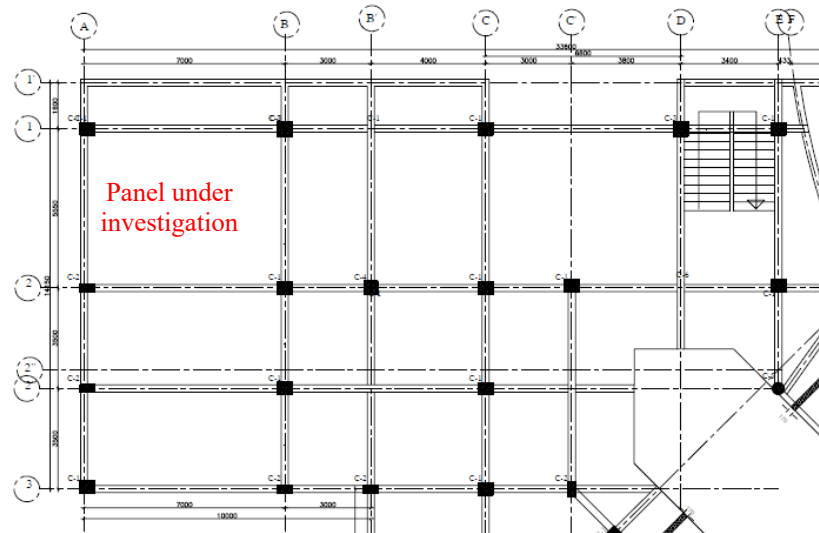


Fig. 2. Typical floor plan of the building

2.1 Construction Information

Materials used for the construction, actual dimensions of the slab, reports on the proportions and properties of the concrete mixtures are checked following ACI 437 standard [16]. Moreover, for the purpose of this study, to get the actual material strengths, tests are performed. The reinforcement steel bar utilized for the work was having a yield strength of 420 MPa and the concrete's average compressive strength of the core was recorded at 24.9 MPa, 26.8 MPa and 29.6 MPa sampled at three different deliveries. The thickness (170mm) and dimension of the slab (center to center spacing of 7m×5.5m) are measured at site. Review of the original design was made in accordance with ES-EN 1992-2015 design code [17]. From the inspection report, it was verified that reinforcing bars are placed as per the original design.

2.2 Equipment and Instruments

Test equipment from the Construction Materials and Structures Laboratory of Addis Ababa Institute of Technology (AAiT) were mobilized. The tools, equipment and instrumentation used for the field test include; Schmidt hammer, core drilling machine, data logger - for digital data acquisition - 500 data points per second, transducers - measurement of vertical displacement (digital), crack scale to measure crack widths, UPS - power storage and power extension cables. The field test is designed to assess the performance of the selected slab and solely targeted on the strength, stiffness, and geometry aspects. In the investigation three tests are carried out; hammer test, core test (compressive strength of concrete) and in-situ load test.

2.2.1 Test set-up

For the test setup, the slab to be investigated was first selected, with existing cracks, damages, or deformations documented. Instrumentation such as displacement transducers (LVDTs) was installed to measure deflections at the mid point and crack width scale was used to measure cracks. Before loading began, initial measurements of deflections, crack widths, and the slab's condition were taken for comparison throughout the testing process. The loading test was conducted using the setup presented in Fig. 3.



Fig. 3. Set-up for loading test (a) slab deflection measurement and (b) data logger

2.2.2 Load intensity

As the slab was already in place (weight of existing slab is 4.25kN/m^2), the superimposed dead load to be applied during the test was determined to be the finishing and design live loads. For the load test, additional dead load of 2.96kN/m^2 ; i.e., weights of cement screed (0.8kN/m^2), floor finish (0.21kN/m^2), ceiling plaster (0.45kN/m^2) and partition walls (1.5kN/m^2), and a live load of 3.0kN/m^2 are considered, resulting in a test load of 6.06kN/m^2 . In this study, a test load of 8.0kN/m^2 was applied to the slab; i.e., 5 layers of cement bags, each weighing 1.60kPa (40qtl with an effective loaded area of $5.75 \times 4.35\text{m}^2$). The slab has a total dead load of 7.21kN/m^2 , which includes the weight of the concrete (4.25kN/m^2) and additional dead loads of 2.96kN/m^2 . The minimum test load required by ACI 318-08 based on Eqn. (1) becomes 12.13kN/m^2 , taking into account γ_D of 1.35 and γ_L of 1.5 as the slab was designed following ES-EN 1992-2015 [17]. Therefore, the load requirement of ACI 318-08 is satisfied, i.e., the total load intensity applied in the slab, including its weight ($12.25\text{kN/m}^2 = 8.0 + 4.25$) was not less than the minimum requirement of 12.13kN/m^2 .

2.2.3 Loading steps and measurements

During the test, the behavior of load-deflection response of the slab was checked at each loading step. The test load was applied incrementally in five layers as recommended by ACI 318 [15] up to the maximum load intensity of 8.0kN/m^2 and deflection is measured using LVDT [16]. In addition to the deflection measurements, any possible cracks formation, opening/closure of flexural cracks were tested and taken after each load increment to monitor the slab's response. The test continued until the slab showed signs of failure, which could include excessive deflection, significant crack widening, material distress (such as spalling or crushing), or instability in the form of a rapid increase in deflection without a corresponding increase in load. Fig. 4 shows a loaded RC slab with cement bags. Finally, the loads are removed immediately after all response measurements (deflection and crack widths) are made. In each loading and testing steps, safety provisions are properly followed.



Fig. 4. Surface loads used for loading test a) three layers b) five layers

3. Results and Discussion

3.1 Crack Formation

Fig. 5 presents the cracks seen on top surface of the deck; they are found to be of random pattern and distributed in the panel fully indicating a non-structural cause i.e., contraction of the paste. The site observations showed that the concrete has been leaking water through the cracks indicating crack opening running deep to the depth of the slab. To confirm this, two core samples were taken at locations where cracks were visible on the surface. The core samples verified that the cracks observed on the top surface extended to the depth of the slab, as illustrated in Fig. 6. For the cracked slab under investigation, a maximum crack width of 0.6mm has been measured.



Fig. 5. Cracks observed at deck top surface



Fig. 6. Core samples reaching the full depth of the slab

Fig. 7 below shows plastic settlement cracks which run along the directions of top restraints. By their nature settlement cracks are known to occur primarily while the concrete is plastic and bleed water is still rising and covering the surface. They tend to roughly follow restraining elements such as reinforcement bars (see Fig. 8) or change in depth of members. To avoid formation of such cracks it is recommended to use mixes with lower bleeding characteristics and increase the ratio of cover depth. Bleed of concrete may result from excessive water to cement ratio (greater than 0.50) or excessive water reducer dosage that causes free water to rise to the top surface. It is also suggested that the finishers wait to proceed until the water evaporates or re-trowel the surface to close the settlement crack openings while the concrete is still plastic.



Fig. 7. Plastic settlement cracks

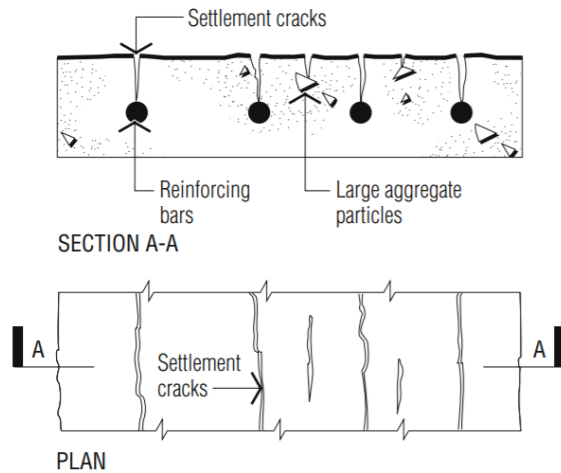


Fig. 8. Settlement cracking concept [18]

Estimation of the water evaporation from the slab surface per area can be made by taking the weather information presented in Table 1 and from the chart presented in Fig. 1. Nevertheless, it is worth noting that the data presented may not be exactly represent the site situation. Data as reported by the National Metrological Data and Climatology Directorate is presented in Table 1 [19].

Table 1. Weather data of Addis Ababa during the concrete casting dates

Date	Maximum temperature (°C)	Minimum temperature (°C)	Rainfall (mm)	Wind speed (m/s)
22	25.7	13.0	0	0.54
23	25.5	11.2	0	0.41

3.1.1 Possible causes of cracks

From the information collected, the concrete slabs on the 2nd floor were casted on February 22 and 23, 2021 and multiple cracks were noticed within 24 hours. These cracks are most likely caused by one or a combination of the following reasons:

- The concrete was casted in February 2021, when the temperature and humidity were 25.5°C and 44%, respectively (which is the maximum temperature and minimum relative humidity in the year 2021). This would have resulted in early aged slab cracking due to rapid and excessive evaporation of water from the concrete.
- Poor cement quality which can also cause a volumetric shrinkage in the produced concrete. However, this cannot be verified without conducting a chemical composition test and physical tests on the cement. No sample of the utilized cement was availed to test its quality neither did the investigators find a report on its quality by the suppliers.
- Problem in mix proportion of concrete: chemical composition and fineness content of cement, excessive use of water to cement ratio, large size of course aggregates and presence of excessive fine aggregates are major causes for early-stage shrinkage cracking. As per the mix design data provided by the contractor, the concrete mix used in this project is in good agreement with the design. However, test results for the constituent materials used for the construction of the slabs were not provided and could not be verified. The reported mix design followed for making C-25 concrete is presented in Table 2.

Table 2. Reported concrete mix design

Weight (kg/m ³)	Water	Cement (OPC 42.5 N)	Fine aggregate	Coarse aggregate (max. size)		Retarding Admixture
				10 mm	20 mm	
	147	335	693	236	767	0.6

The specific materials used in making the concrete were said to have been fully utilized, making it impossible to extract samples for additional laboratory investigations.

- iv. The contractor may not have used the proper slab curing procedure. As a result of this, excessive evaporation of water from the concrete was accelerated and hence the section has cracked. Rapid drying of the surface of the concrete due to high temperature caused the slab to shrink and crack. Further drying shrinkage resulted a full-depth cracking of the concrete slab which propagated to the slab soffit.

3.1.2 Investigation of curing condition

Beam and column curing involved the application of water sprinkling, while wet burlap was used to cover the slabs. However, based on site observations the assurance of consistent burlap saturation through intermittent sprinkling was lacking. Inadequate moisture distribution caused by inconsistent burlap saturation could have resulted in non-uniform curing of the concrete. This non-uniform curing possibly contributed to differential shrinkage and stress within the concrete, which in turn increased the likelihood of cracks forming. Moreover, insufficient moisture during curing likely caused the surface of the concrete to dry out too quickly, leading to surface cracks.

3.1.3 Core strength

The strength of the core was made in accordance with testing procedures of ACI 214.4R-03 [20] and the results showed that the cylindrical strength of the samples complies with the design strength of concrete.

3.2 Performance Assessment of RC Slab

Structural performance assessment can be carried out using a deterministic or probabilistic approach. A deterministic analysis is a conservative method of assessment that determines whether or not the structure is safe by taking mean values of all variables with the appropriate factors mentioned in the codes [21–23]. On the other hand, a reliability-based analysis of structures is challenging as there are lack of design information and uncertainties in random variables [21,23,24].

3.2.1 Deterministic analysis

In this section, design review and performance assessment process of the slab under investigation is made deterministically. First, the design was checked using an Extended Three-Dimensional Analysis of Building System (ETABS V21.1.0 [25]) software and the results are compared with the actual drawings used in the construction. The summary of design review output is shown in Fig. 9 and the results are summarized in Table 3.

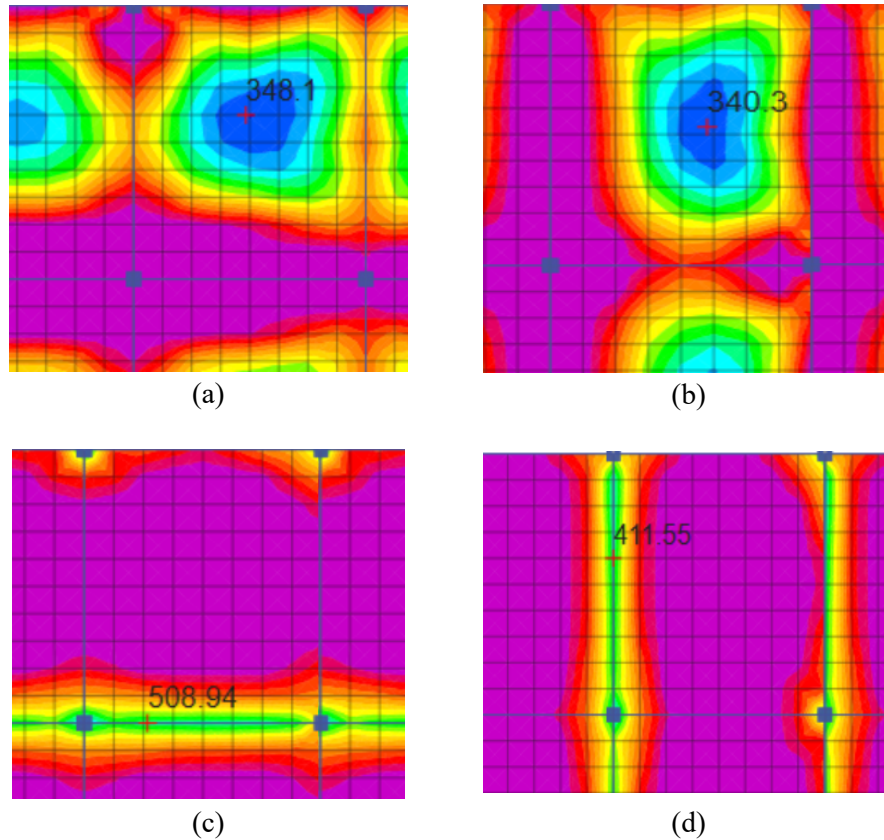


Fig. 9. Rebar intensity (mm^2/m) (a) bottom, x- direction (b) bottom, y-direction (c) top, x- direction and (d) top, y-direction

Table 3. Review of reinforcements in slab

Description	Reinforcement areas (mm^2/m)			
	Support		Span (field)	
$A_{s,\text{required}}$ (mm^2/m)	506.94	411.55	348.10	340.30
$A_{s,\text{provided}}$ (mm^2/m)	628.15	628.15	650.10	417.25

As shown in Table 3, the actual reinforcements provided in the construction of the 2nd floor slab satisfy the requirement and are adequate. Moreover, material properties used in the construction are in line with the design values. The section capacity for the defective slab was carried out using a finite element tool, SHELL-2000 (Reinforced Concrete Sectional Analysis using the Modified Compression Field Theory). The geometric and material characteristics are taken from design data and field test results. Fig. 10 below shows the geometric and material properties of the defective slab. The section is analyzed for its moment capacity for both in the x- and y- directions. The output of the software is shown in Fig. 11. In the analysis, as the concrete was cracked at its early stage, shrinkage and temperature strains are also considered. The evaluation of the RC slab's flexural capacity is summarized in Table 4, where it is evident that the capacity to demand ratio is greater than one, indicating that the slab has no substantial structural deterioration and has enough resistance to flexural action as indicated in ACI 562 [26].

Table 4. Assessment of flexural capacity of RC slab

Moment (kN-m/m)	M_{xf}	M_{yf}
Design moment, demand (1)	17.60	12.90
Section capacity (Software output)	25.77	19.33
Design capacity, (multiplied by 0.9) (2)	23.19	17.40
Capacity to demand ratio (2)/(1)	1.32	1.35

Shell Properties		
	X-Dir'n	Y-Dir'n
A_s (mm ² /m)	417	650
ρ (percent)	0.245	0.382
ρf_y (MPa)	1.04	1.78
Crack Space (mm)		

Concrete shrinkage strain:
0.00 mm/m

Loading (Constant + Increment)
0.00, 0.00, 0.00, 0.00, 0.00, 0.00, 0.00, 0.00 +
0.00, 0.00, 0.85, 1.00, 0.75, 0.00, 0.00, 0.00

Concrete

Rebar

X-Reinforcement: $A_s = 50 \text{ mm}^2 @ 120 \text{ mm } 24 \text{ mm up}$

Y-Reinforcement: $A_s = 78 \text{ mm}^2 @ 120 \text{ mm } 20 \text{ mm up}$

All dimensions in millimetres
Minimum clear cover : 25 mm

DEC: RC defective Slab

AAiT

(a)

Concrete Properties

Type List: Concrete

Defined Types: Concrete

Base Curve: Popovics/Thorenfeldt/Collins

Comp. Softening: Vecchio-Collins 1986

Tension Stiffening: Bentz 1999

Steel Properties

Type List: x-steel, y-steel

Defined Types: x-steel, y-steel

Predefined Type: Custom type

Concrete Details

Cylinder Strength: 27.1 MPa (eg: 35.0)

Tension Strength: Auto 1.68 MPa (eg: 2.00)

Peak Strain: 2.45 mm/m (eg: 2.00)

Aggregate Size: 10 mm (eg: 20)

Tension Stiff Factor: 1.0 (eg: 1.0)

Rebar Details

Elastic Modulus: 200000 MPa (eg: 200000)

Yield Strength: 425 MPa (eg: 400)

e-Strain Hardening: 8.0 mm/m (eg: 20.0)

Rupture Strain: 100 mm/m (eg: 100)

Ultimate Strength: 425 MPa (eg: 600)

(b)

Fig. 10. (a) Geometric properties and (b) Material properties for concrete and steel

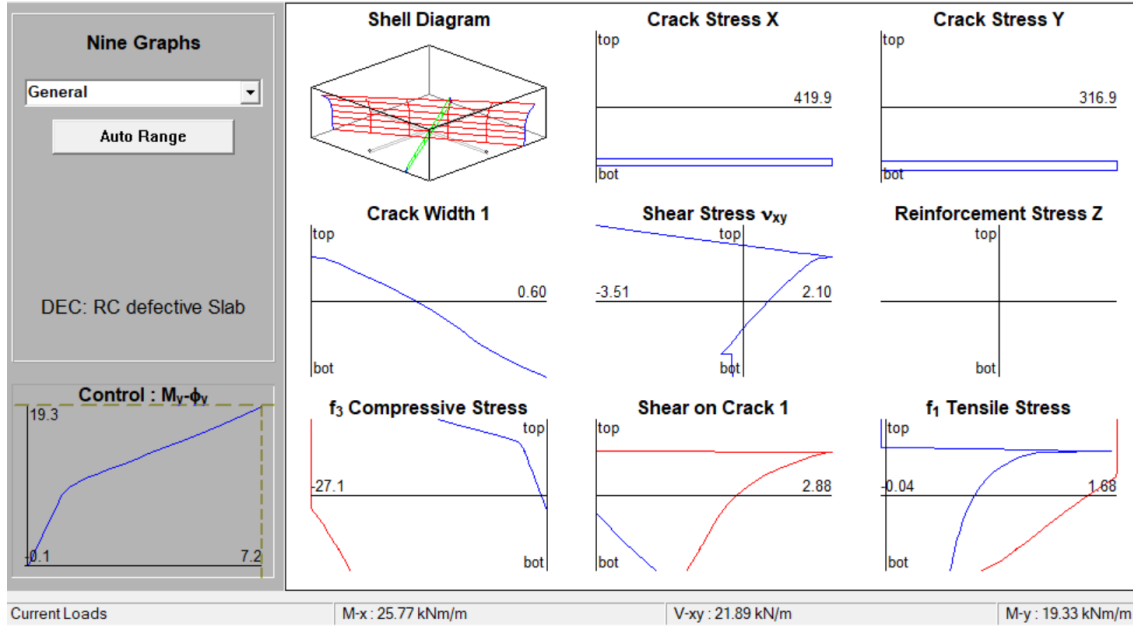


Fig. 11. Analysis Output

3.2.2 Reliability analysis

A reliability analysis of the cracked slab under investigation is done by considering different variations in material properties (especially compressive strength of concrete and yield strength of reinforcing bars), concrete overlay (floor finish), live loads and etc. Furthermore, as construction errors affect section capacity, errors in its section dimensions are considered which accounts the defects in construction caused by lack of skilled manpower and quality of formworks [27]. In a general case, the probability of failure P_f is defined by the limit state function, $g(x) < 0$ and it is given in Eq. (4) [28]:

$$P_f = P(g(x) < 0) \quad (4)$$

where P_f is the probability of failure, $g(x)$ is the limit state function, design margin = $R(x) - S(x)$, $R(x)$ is the resistance of the section and $S(x)$ is effect of loads. Since bending resistance has a lognormal (LN) distribution and load effects have normal (N) distributions [29], the reliability index of the structure is estimated using Rackwitz and Flessler expressions given in Eqs. (5) and (6), respectively [30].

$$\beta = \frac{\mu_R \left(1 - k \frac{\sigma_R}{\mu_R}\right) \left[1 - \ln \left(1 - k \frac{\sigma_R}{\mu_R}\right)\right] - \mu_S}{\sqrt{\left(\mu_R \left(1 - k \frac{\sigma_R}{\mu_R}\right) \left(\frac{\sigma_R}{\mu_R}\right)\right)^2 + \sigma_S^2}} \quad (5)$$

$$k = (\bar{R}^e - r^*) / \sigma_R^e \quad (6)$$

where β is the reliability index, μ_R , σ_R are mean and standard deviation of the resistance, respectively, μ_S , σ_S are mean and standard deviation of total-load effect, respectively, \bar{R}^e , σ_R^e are mean and standard deviation for the resistance of the approximating normal distributions (equivalent normal parameters), respectively, k is a multiplication factor of the standard deviation, and r^* is a design point on the failure boundary.

Table 5. Statistical distribution of random variables

No.	Random variables	Mean values	CoV (%)	Std. dev.	Distribution	References
1	Yield strength for flexural reinforcement steel, f_y (MPa)	420	5	21	LN	[21,27,29,32]
2	Cylindrical compressive strength of concrete, f'_c (MPa)	27	10	2.7	LN	[29,32]
3	Longitudinal bars x-direction, A_{sx} (mm ² /m)	650	2	13	N	[29]
4	Longitudinal bars y-direction, A_{sy} (mm ² /m)	417	2	8.3	N	[29]
5	Live load	1.00	25	0.25	N	[23,29,32]
6	Permanent loads (finishing and partition loads)	1.00	10	0.10	N	[23,29]
7	Analysis Variable for DL and LL; Av_{dl} and Av_{ll}	1.00	5	0.05	LN	[29,33]
8	Resistance factor, ϕ	0.90	10	0.09	N	[29]
9	Model uncertainty for the resistance and load effects, N_R	1.00	4.6	0.046	LN	[29]
10	Slab thickness, t_s (mm)	170	0.5	0.85	N	[29,32]
11	Concrete cover, c (mm)	15	10	1.50	N	[23]

The statistical variations of random variables considered in this study is shown in Table 5. Their statistical distributions are obtained from literatures, standards, codes and manuals [21,23,27,29,31–33].

To determine the number of possible combinations of random variables, Latin Hypercube Sampling (LHS) method is used. LHS method is selected as it permits a limited number of simulations with acceptable level of accuracy [21]. The number of possible combinations is computed using Eq. (7) [34,35].

$$n = 2^k \quad (7)$$

where n is the number of possible combinations (runs), k is the number of input variables, and it is a power of 2; ($k = 2^m$) and m is an integer.

Table 4 considers 11 input variables (k) where m varies from 3 to 4, resulting in k values of 8 and 16. The possible combinations of random variables should not be less than $2^8=256$ [34]. This satisfies the minimum number of samples required by [36], which specifies that the sample size must be at least four times the number of input random variables (in this study, it is $44 = 4 \times 11$) if the correlation algorithm is used. Hence, in this study, using a built-in LHS design function in MATLAB with mean and standard deviation criterion, LHS of 11 factors (random variables) in 256 combinations is generated [37] and some of which are shown in Table 6. The data is filtered from erroneous combinations using the concept of constrained LHS [38,39], i.e., for instance, the flexural resistance factor (strength reduction factor, ϕ) as specified in [15] does not exceed one.

Table 6. LHS of 11 factors in 256 runs

<i>runs</i>	<i>Random variables (factors)</i>										
	f'_c	f_y	NR	A_{sx}	A_{sy}	LL_f	DL_f	A_{vll}	ϕ	t_s	c
1	26.25	426.15	1.02	638.93	412.70	0.88	0.99	1.05	0.83	169.69	12.67
2	24.06	398.27	0.93	635.41	417.69	0.81	0.91	0.99	0.87	169.09	11.84
3	24.30	427.23	1.01	647.91	406.34	1.17	1.10	1.02	0.95	168.87	11.50
4	29.95	380.31	1.00	638.18	413.88	0.95	1.08	0.98	0.94	169.83	14.29
⋮											
256	23.62	382.14	0.96	633.31	416.02	0.97	1.05	0.89	0.90	170.60	16.21

The probabilistic assessment results in terms of design margin for bending moment in x- and y-directions are computed and the corresponding probabilistic distribution graphs are presented in Fig. 12. The reliability indexes of the slab under investigation for bending moments in x- and y- directions are computed using Eqn. (5) and they are found to be 5.52 (β_{Mx}) and 4.17 (β_{My}), respectively. Thus, the safety index of the slab structure becomes 4.17 with a probability of failure of 10^{-6} [21]. The slab is found to fulfill the minimum requirements for ultimate limit states with medium consequence of failure (office and public buildings), with a reliability index limit of 3.8 (for a 50-year return period) [21,40]. Furthermore, it satisfies the minimum target reliability index requirement of 2.5 for a slab element subjected to bending [41].

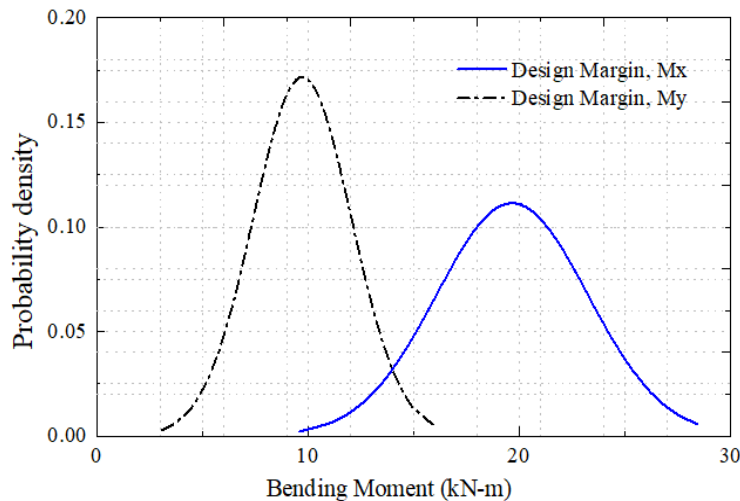


Fig. 12. Probabilistic distribution of design margin for moment

3.3 Verification of capacity of slab by load test

3.3.1 Load deflection results

Time-history and record of mid-span deflection of RC slab due to external surface loads are shown in Figs. 13 and 14, respectively. From Fig. 14, under the action of various loading steps, it is observed that the load-displacement relationship is linear and no opening or closure of cracks have been noticed. As there was no nonlinear load-deflection was observed at each loading step, the slab was loaded up to the maximum load (8kN/m^2). As can be observed from the deflection curve of the RC slab, the structure's deflection due to additional dead and live loads (6.06kN/m^2) was found to be 6.81mm. The deflection of the slab for 5 layers of surface load was measured as 8.68 mm.

The maximum deflection of the slab, computed from Eqn. (2) becomes 8.89 mm [15]. In all cases,

the deflection limit is not exceeded making the slab is reasonably safe against serviceability and strength requirements. The result showed that the slab is verified to be safe as it achieved to resist the desired load of 8 kN/m^2 . Furthermore, it was observed that, the residual deflection of the beam after removal of the test loads was measured as 0.71 mm . This is one-third of the residual deflection limit ($=2.23 \text{ mm}$), which was computed using Eqn. (3). It shows that there was “no evidence of failure” as more than 90% of the deflection of the slab was recovered [15]. As a result, even with cracks, the structure's strength is satisfactory.

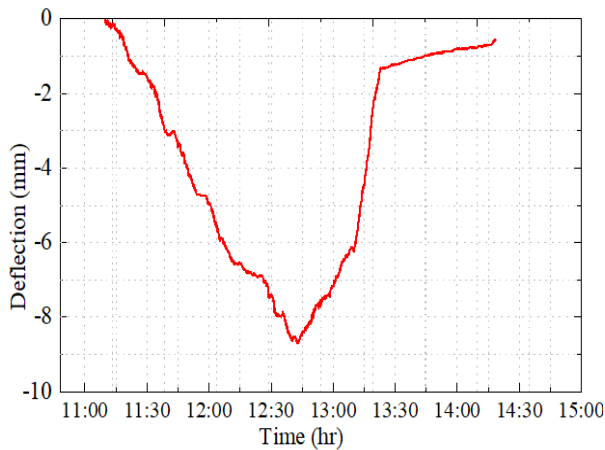


Fig. 13. Time-history of deflection

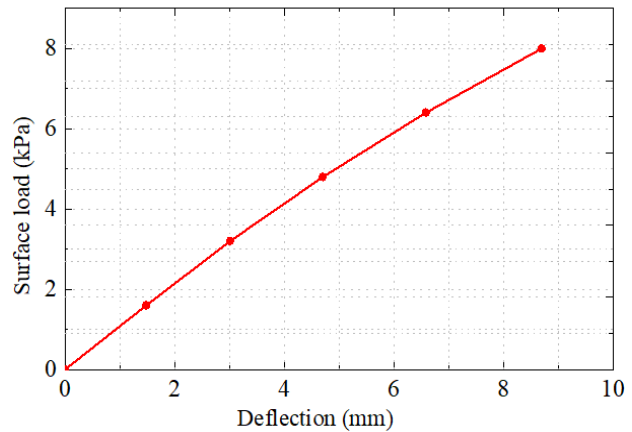


Fig 14. Mid-point deflection under surface loads

3.3.2 Crack widths

During the load test, it was observed that the behavior of the cracks remains unchanged and no further movement of cracks was visualized (no opening and closure of cracks: stabilized cracks). Thus, the cracks are classified as non-structural cracks and there will not be durability issues of the structure, if they are properly treated.

4. Conclusions

Even if the RC slab under investigation has many cracks, “no evidence” of failure was observed. The adequacy of the slab was verified using numerical analysis and a full-scale load test. Hence, the defective reinforced concrete slab is safe against stiffness and strength limits. An overlay with the intended thickness indicated in the original drawing is to be constructed by placing mortar over a cracked concrete surface, and ACI 224R [42] application procedures should be followed. Alternate suitable filler materials should also be used before applying finishing materials to the cracked slab and the cracks should not be left untreated.

The findings of this study provide critical insights into the structural performance of damaged slabs under real-world conditions. By assessing the slab's ability to carry loads in a damaged state, this research highlights the impact of cracks and other imperfections on structural integrity, and helps establish whether repairs or reinforcements are needed to maintain safety and functionality. The results can also influence design guidelines for dealing with pre-existing damage in concrete structures, suggesting that certain levels of damage may still allow the structure to meet safety standards. This research offers a valuable tool for civil engineers, structural inspectors, and facility managers who are responsible for assessing the condition of aging or damaged structures. In-situ load testing can be applied to buildings, bridges, and other critical infrastructure to determine whether they can continue to be used safely without costly, large-scale interventions. This method

can also be used to validate the effectiveness of repairs or retrofitting by comparing pre- and post-repair load-carrying capacity. It's particularly useful in situations where visual inspections or non-destructive testing alone are not sufficient to assess the true condition of the slab.

The study advances the understanding of how in-situ load testing can be applied in practical settings, especially in scenarios involving damaged or cracked slabs. It contributes to the body of knowledge by demonstrating how this method can be used not only to evaluate structural capacity but also to monitor the progression of damage under load. Additionally, it offers a framework for using numerical simulations alongside experimental data to provide more comprehensive evaluations of concrete structures. The research also underscores the importance of developing tailored guidelines for in-situ load testing in damaged conditions, potentially influencing future building codes and standards. Future research is recommended to focus on the influence of loading conditions and the long-term monitoring and performance evaluation of cracked RC slabs.

Conflict of Interest

The authors declare that there is no conflict of interest.

Acknowledgments

This study was undertaken in the School of Civil and Environmental Engineering, Addis Ababa Institute of Technology. The authors gratefully acknowledge Ms. Kalkidan Tesfaye for her professional assistance in conducting the load test.

Author Contributions

Yisihak Gebre: Concept, Design the structure, Methodology, Writing the manuscript, Performed the analysis, and Revision of the manuscript.

Biruktawit Taye: Concept, Collected the data, Methodology, and Designed the analysis.

Abrham Gebre: Concept, Design the structure, Collected the data, Writing sections 3.1 and 3.2, Designed the analysis, Performed the analysis and Revision of the manuscript.

Asmerom Weldegerima: Collected the data, Methodology, Analysis and Revision of the manuscript.

References

- [1] Mehndi, S. M., Khan, M. A., Ahmad, S., Causes and Evaluation of Cracks in Concrete Structures. *International Journal of Tech. Research and Applications*, 2(5), 29-33, 2014.
- [2] Sayahi, F., Plastic Shrinkage Cracking in Concrete: Mitigation and Modelling. Doctoral Thesis, Luleå University of Technology, Department of Civil, Environmental and Natural Resources Engineering, Luleå, Sweden, 2019.
- [3] ACI 305R-20, Guide to Hot Weather Concreting. *American Concrete Institute*, ACI Committee-305, 1999.
- [4] Thanoon, W. A., Jaafar M. S., Kadir, M. R. A., Noorzaei, J., Repair and Structural performance of initially cracked reinforced concrete slabs. *Construction and Building Materials*, 19(8), 595-603, 2005.

- [5] De Luca, A., Zadeh, H. J., Nanni, A., In-situ Load Testing of a One-Way Reinforced Concrete Slab as per ACI 437 Standard. *Journal of Performance of Constructed Facilities*, 28 (5), 04014022, 2014.
- [6] Dmochowski, G., Berkowski, P., Schabowicz, K., Wójcicki, Z., Grosel, J., Dłucik, Ł., Failure Analysis of RC Floor Slab in Industrial Hall. In *Modern Building Materials, Structures and Techniques. Proceedings of the International Conference*, Vilnius Gediminas Technical University, 10, p.587, 2010.
- [7] Saleem, M. A., Abbas, S., Nehdi, M. L., Assessment of Reinforced Concrete Slabs Using In-situ Load Testing: A Case Study. *Journal of Building Engineering*, 25, p.100844, 2019.
- [8] Ziehl, P. H., Galati, N., Nanni, A., Tumialan, J. G., In-situ Evaluation of Two Concrete Slab Systems. II: Evaluation Criteria and Outcomes. *Journal of Performance of Constructed Facilities*, 22(4), 217-227, 2008.
- [9] Abu-Khajil, A., Reliability Assessment of Load Testing for Concrete Buildings. M.Sc Thesis, University of Waterloo, Ontario, Canada, 2015.
- [10] Calisang, S.R., Non-destructive Evaluation of an Existing Concrete Structure using Load Test. *International Journal of Scientific Engineering and Research (IJSER)*, 6(11), 63-71, 2018.
- [11] Casadei, P., Parretti, R., Nanni, A., Heinze, T., In situ Load Testing of Parking Garage Reinforced Concrete Slabs: Comparison between 24 h and Cyclic Load Testing. *Practice Periodical on Structural Design and Construction*, 10(1), 40-48, 2005.
- [12] Matysek, P., Witkowski, M., Analysis of the Causes of Damage to the RC Floor Slab in the Underground Garage, *MATEC Web of Conferences*, 284, p. 06004, 2019.
- [13] Galati, N., Nanni, A., Gustavo, T. J., Ziehl, P. H., In-situ Evaluation of Two Concrete Slab Systems. I: Load Determination and Loading Procedure. *Journal of Performance of Constructed Facilities*, 22(4), 207-216, 2008.
- [14] Gold, W.J., Nanni, A., In-situ Load Testing to Evaluate New Repair Techniques. In *Proc., NIST Workshop on Standards Development for the Use of Fiber Reinforced Polymers for the Rehabilitation of Concrete and Masonry Structures*, 102-112, 1998.
- [15] ACI 318. Building Code Requirements for Structural Concrete (ACI 318-08) and Commentary, *American Concrete Institute*, 2008.
- [16] ACI 437R. Strength Evaluation of Existing Concrete Buildings. *American Concrete Institute*, ACI Committee-437, 2019.
- [17] ES EN 1992-1-1:2015. Design of Concrete Structures- Part 1-1: General Rules and Rules for Buildings. Ministry of Construction, Addis Ababa, Ethiopia, 2015.
- [18] Plastic Settlement Cracking. Cement Concrete & Aggregates Australia (CCAA), Data Sheet, Australia, 2005.
- [19] http://www.ethiomet.gov.et/data_access/information, accessed on May 02, 2024.
- [20] ACI-214.4R. Guide for Obtaining Cores and Interpreting Compressive Strength Results.

American Concrete Institute, ACI Committee-214, 2003.

- [21] Rücker, W., Hille, F., Rohrmann, R., Guideline for the Assessment of Existing Structures, *Federal Institute of Materials Research and Testing*, Final Report-F08a, 2006.
- [22] Gebre, A., Gebreyouhannes, E., Gebre, Y., Probabilistic Assessment and Field Test Verification for Strength Evaluation of Bridge with Defective Girder. *Zede Journal of Ethiopian Engineers and Architects*, 41(1), 17-28, 2023.
- [23] Muhammed, J. J., Deterministic and Probabilistic Approaches in the Analysis of the Bearing Capacity of a Bridge Foundation on Undrained Clay Soil. *Slovak Journal of Civil Engineering*, 27(2), 44-51, 2019.
- [24] Rezaee, R., Brown, J., Augenbroe, G., Kim, J., Assessment of Uncertainty and Confidence in Building Design Exploration. *AIEDAM*, 29(4), 429-441, 2015.
- [25] ETABS V21.1.0. Structural and Earthquake Engineering Software. *Computers and Structures, Inc. (CSI)*, 2023.
- [26] ACI 562-19. Code Requirements for Assessment, Repair, and Rehabilitation of Existing Concrete Structures. *American Concrete Institute*, 2019.
- [27] Seo, D., Shin, S., Han, B., Reliability-based Structural Safety Evaluation of Reinforced Concrete Members. *Journal of Asian Architecture and Building Engineering*, 9(2), 471-478, 2010.
- [28] Nguyen, H. A. T., Probabilistic Assessment of Bending Strength of Statically Indeterminate Reinforced Concrete Beams. *International Journal of Engineering*, 35(4), 837-844, 2022.
- [29] Van Coile, R., Caspeelee, R., Taerwe, L., The Mixed Lognormal Distribution for a More Precise Assessment of the Reliability of Concrete Slabs Exposed to Fire. *Proceedings of ESREL*, 29(9), 02-10, 2013.
- [30] Rackwitz, R., Flessler, B., Structural Reliability under Combined Random Load Sequences. *Computers & Structures*, 9(5), 489-494, 1978.
- [31] ACI 214R. Guide to Evaluation of Strength Test Results of Concrete. *American Concrete Institute*, ACI Committee-214, 2011.
- [32] ASCE-02. Minimum Design Loads for Buildings and other Structures, *American Society of Civil Engineers*, 2nd edition, 2002.
- [33] Tarekegn, A. G., Time-Dependent Reliability Analysis for Deflection of a Reinforced Concrete Box Girder Bridge. *International Journal of Engineering and Applied Sciences*, 15(2), 60-74, 2023.
- [34] Steinberg, D. M., Lin, D. K., A Construction Method for Orthogonal Latin Hypercube Designs. *Biometrika*, 93(2), 279-288, 2006.
- [35] Cronvall, O., Structural Lifetime, Reliability and Risk Analysis Approaches for Power Plant Components and Systems. *VTT Publications 775*, Finland, 2011.
- [36] Fleming, J., Manteufel, R., Replicated Latin Hypercube Sampling. In *46th*

AIAA/ASME/ASCE/AHS/ASC Structures, Structural Dynamics and Materials Conference, American Institute of Aeronautics and Astronautics, p.1819, Austin, Texas, 2005.

- [37] MATLAB. Programming Language, R2021a. The MathWorks, Inc., Natick, Massachusetts, USA, 2021.
- [38] Shields, M. D., Zhang, J., The Generalization of Latin Hypercube Sampling. *Reliability Engineering & System Safety*, 148, 96-108, 2016.
- [39] Petelet, M., Iooss, B., Asserin, O., Lored, A., Latin Hypercube Sampling with Inequality Constraints. *AStA Advances in Statistical Analysis*, 94, 325-339, 2010.
- [40] Stanojev, M. L., Stojic, D., Reliability Analysis of Structures. *Facta Universitatis, Series: Architecture and Civil Engineering*, 12(3), 265-272, 2014.
- [41] Viegas, C. H. H., Real, M. D. V., Reliability Analysis of Reinforced Concrete Slabs Designed according to NBR 6118. *International Journal of Advanced Engineering Research and Science (IJAERS)*, 9(7), 286-297, 2022.
- [42] ACI 224-R. Control of Cracking in Concrete Structures. *American Concrete Institute, ACI Committee-224*, 2001.

Deflections of Cantilever Beams Subjected to A Point Load at the Free End

Alper Oğulcan Söylemez ^a, Bekir Akgöz ^{b*}

^{a,b} Department of Civil Engineering, Faculty of Engineering, Akdeniz University, Antalya, Türkiye

✉: bekirakgoz@akdeniz.edu.tr^{b*}, soylemezalperogulcan@gmail.com^a : 0009-0000-5352-4316^a, 0000-0003-2097-2555^{b*}

Received: 01.08.2024, Revised: 25.10.2024, Accepted: 01.11.2024

Abstract

In this study, the displacements of cantilever beams for various slenderness ratios under point load are analyzed using Timoshenko and Bernoulli-Euler beam theories. The variation of the slenderness ratio is achieved only by changing the beam length. The results from these theories are compared with those from SolidWorks, which is considered a reliable simulation software. With this comparison, the % difference rates between the simulation and theoretical results are determined. This study explains under which conditions the Timoshenko and Bernoulli-Euler beam theories should be applied and evaluates the accuracy of the simulation software. Detailed research is carried out to examine its compatibility with these two theories. Some numerical results are presented to demonstrate their validity and sensitivity.

Keywords: Beam bending, Timoshenko beam theory, Bernoulli-Euler beam theory, SolidWorks.

1. Introduction

Beams are one of the bar elements frequently used in civil engineering and building design. Beams, which are one-dimensional structural elements, are generally in vertical and horizontal positions and are exposed to loads in the direction of the bar axis and perpendicular to the bar axis. To give examples of places where they are used, we can give some examples such as buildings and bridges. However, it is possible to see objects modeled as beams in many parts of life. For example, the working principle of the atomic force microscope (AFM) can be given as an example of a cantilever beam (see Fig. 1).

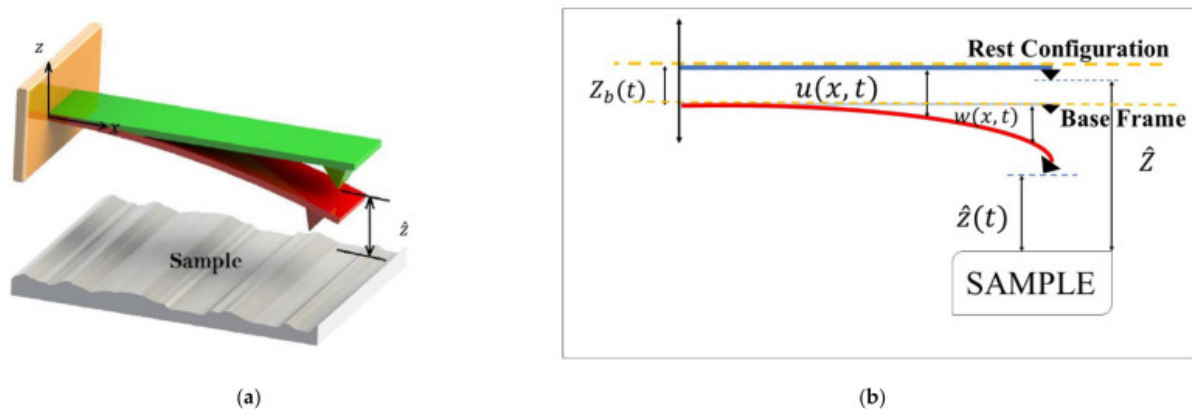


Fig. 1. The schematic view of an AFM's cantilever scanning a sample. a) 3D view of the AFM. b) 2D view of the cantilever [1].

The behavior of these elements under loads is of great importance for the safety, durability, and design of structures. Being able to analyze these behaviors accurately is essential for beams to be designed both safely and efficiently. Significant studies have been carried out on this subject from the past to present. The oldest known study among these studies was carried out by Leonhard Euler in 1744 [2]. In this study, Euler examined the displacements and buckling of beams and used algebra of variation to obtain these equations. Over the following years, this study became the pioneer of many studies to follow. Detailed information about these and the historical development of elastic stability can be found in the book “Theory of Elastic Stability” by Timoshenko and Gere [3]. There is also a study on the mechanics of materials by Gere and Timoshenko, which includes the theory of bending and displacement of beams [4]. Apart from these studies, quite extensive studies have been carried out. For example, Wang et al. [5] provide definitive solutions for buckling analysis of structural elements and aims to solve common problems in engineering structures by analytical methods. Zienkiewicz et al. [6] made a comprehensive resource on the finite element method (FEM), and this resource discusses the basic principles and applications of FEM in detail and explains how this method can be used to solve engineering and scientific problems. Bazant [7] addressed a comprehensive book that covers the basic principles of stability analysis, explaining in detail the various theories used to study the stability of structural members. Ghali et al. [8] is a comprehensive resource that combines classical and matrix methods used in structural analysis. Cook et al. [9] comprehensively explained the basic principles, mathematical foundations, and use of FEM in engineering practices and show how to use the finite element method in solving engineering problems [9]. While Akgöz et al. [10, 11] explained how to use Bernoulli-Euler beam model in the bending analysis of single-walled carbon nanotubes, in another study they presented a discrete singular convolution method for calculating the deflection analysis of beams resting on elastic foundations. Van Vinh et al. [12] investigated the static bending and buckling behaviors of bi-directional functionally graded (BFG) plates with porosity. Yaylacı et al. [13] carried out a numerical investigation on the vibration and buckling of functionally graded material (FGM) beam containing edge crack using FEM and multilayer perceptron (MLP) [13]. Azizi et al. [14] conducted a study to find deflection of a beam using finite element method based on Bernoulli-Euler and Timoshenko beam theories. Oladejo et al. [15] compared the results of deflection analysis of cantilever beam with COMSOL program to show its accuracy. Chaphalkar et al. [16] described the experimental apparatus and the associated theory which allows to obtain the natural frequencies and modes of vibration of a cantilever beam. Also, all the frequency values are analyzed with the numerical approach method by using ANSYS finite element package has been used. Hodzic [17] described the bending of cantilever beam and its analysis using finite element method. He compares the results obtained for boundary conditions with the results obtained from ANSYS simulation program. Raj et al. [18] conducted a study on modelling, simulation and analysis of cantilever beams by using ANSYS & MATLAB and theoretically by FEM for the evaluation of natural frequency and mode shape. Quang et al. [19] analyzed a three-span continuous beam using FEM and ANSYS via GUI method and APDL parameters. Ho et al. [20] compared the experimental results on deflection values of aluminum beam with the results calculated by FEM. SolidWorks 3D CAD software is used to build the beam model and perform finite element analysis. Samal et al. [21] investigated the deflection and stress distribution in a long, slender cantilever beam of uniform rectangular cross section made of linear elastic material properties that are homogeneous and isotropic. Finite element analysis of the beam was done considering various types of elements under different loading conditions in ANSYS 14.5. Balart Gimeno et al. [22-24] conducted some studies using the finite element method and the SolidWorks program. Onimowo [25] investigated the deflection and bending stress in a cantilever beam having a uniform rectangular cross section with a point load using a 3D Finite Element (FE) model. The results are validated using Bernoulli-Euler’s elastic curve theory equations. Ya et al. [26] calculated the deflection of a cantilever beam was simulated under the action of uniformly distributed load. Then, compared the results obtained from the

simulation with the results of Artificial Neural Networks (ANN). Talebi Rostami et al. [27] analyzed a Timoshenko beam with snowflake cross-section for different boundary conditions and variable properties. The equation of motion was solved with FEM and compared with the SolidWorks simulation. Gao [28] carried out deflection analysis of beams with the help of COMSOL program according to the finite element method and compared it with the results obtained from Timoshenko and Bernoulli-Euler beam theory. Onwubolu [29] presented to be an important resource for today's studies with his book on the use of SolidWorks.

As mentioned above, many studies have been carried out on this subject to date, since the concept of displacement has a decisive role in the design of structural elements exposed to loads. In this study, Bernoulli-Euler and Timoshenko beam theories will be compared for beams with different slenderness ratios that change as the cross-section changes along the beam length. Then, these results will be compared with SolidWorks, one of the simulation programs widely used in engineering design.

Bernoulli-Euler beam theory is one of the best-known and most used theories in engineering. This theory was developed by Jakob Bernoulli and Leonhard Euler in the 18th century. This beam theory is also known as thin beam theory or engineering beam theory. In Bernoulli-Euler beam theory, collapse and load-carrying behaviors are calculated. There are some assumptions in Bernoulli-Euler beam theory. In the approach of the Bernoulli-Euler beam theory, each beam section is perpendicular to the beam axis in case of bending. Bernoulli-Euler beam theory is independent of y -axis [30]. Therefore, the stresses in y -axis are neglected and the beam is assumed to have a straight axis. Due to these assumptions, Bernoulli-Euler beam theory is a simple beam theory to solve and use. Due to these negligible values, applying Bernoulli-Euler to beams with a high slenderness ratio will give us more accurate options. Because shear deformation and moment of inertia effects are less effective in beams with a high slenderness ratio.

Timoshenko beam theory was presented by Stephen Timoshenko in the early 20th century [31]. This beam theory has been one of the most widely used beam theories since it was presented. This is because, in addition to Bernoulli-Euler beam theory, it also uses values of shear deformation and moment of inertia due to shear force. Therefore, Timoshenko beam theory can be considered as an advanced version of the Bernoulli-Euler beam theory. Due to the shear deformation and moment of inertia values taken into calculation in the Timoshenko beam theory, it is expected that the Timoshenko beam theory will always give more accurate results than the Bernoulli-Euler beam theory. The deformed shapes of these two beam models are depicted in Fig. 2.

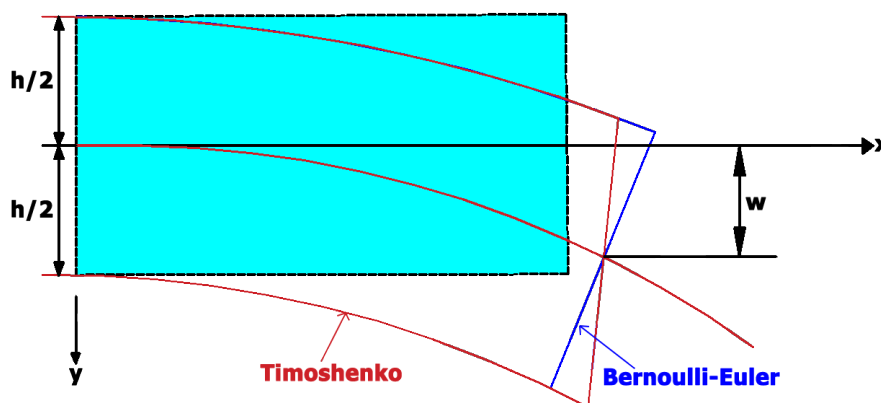


Fig. 2. Comparison of Timoshenko and Bernoulli-Euler beam deformations

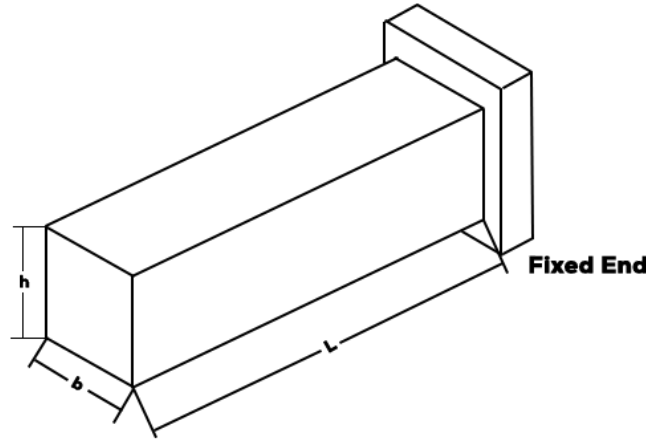


Fig. 3. Cantilever beam with rectangular cross-section

A schematic configuration of a cantilever beam with length L , height h , and width b is shown in Fig. 3. Timoshenko beam theory is also known as first-order shear deformation beam theory because it gives better results in such thick beams compared to Bernoulli-Euler beam theory. So, Bernoulli-Euler and Timoshenko beam theories are the two main approaches used in the deformation analysis of beams and have their advantages and disadvantages. Bernoulli-Euler beam theory is widely preferred because of its simplicity of solution and its realistic results on long beams. However, Bernoulli-Euler beam theory cannot provide sufficient accuracy for short and thick beams because it neglects shear deformation and moment of inertia. Although the Timoshenko beam theory involves a more complex mathematical solution, it gives more accurate results with the values of shear deformation and moment of inertia included in the calculation. Comparing the performances of these two theories on beams with different slenderness ratios is important to determine which theory is more suitable for engineering and structural design. Comparison of these two beam theories with the analysis and simulation software widely used in today's engineering applications will help us to see the compatibility between the theories and the software packages.

In this study, SolidWorks is chosen as the software to compare the theories. SolidWorks is a widely used software in engineering design. SolidWorks can perform detailed analysis of beams with complex geometries and load conditions using FEM. The simulation tools offered by SolidWorks provide the opportunity to analyze the behavior of beams under static and dynamic loads in detail. This study aims to examine how compatible SolidWorks simulations are with the theoretical results obtained with Bernoulli-Euler and Timoshenko beam theories. Particularly, which theory is more appropriate to use in displacement analyses of beams with different slenderness ratios, by comparing these theories with SolidWorks results, the validity and accuracy of the theories in practical applications will be tested. The results of the study will be a guide to providing more effective and reliable solutions in beam design.

2. Theory and Formulation

As shown in Fig.4, when a point load (P) of 1000 N is applied to a homogeneous cross-section cantilever beam with constant material properties from its non-fixed end, the displacement value according to Bernoulli-Euler beam theory can be expressed as follows:

From the moment-curvature relationship, we know that:

$$-EI \frac{d^2 w}{dx^2} = M(x) \quad (1)$$

where E is the modulus of elasticity, I is the moment of inertia, and $M(x)$ is the bending moment at a distance x , and $\frac{d^2w}{dx^2}$ is the curvature of the beam. The bending moment at a distance x from the free end is given by, $M(x) = -Px$.

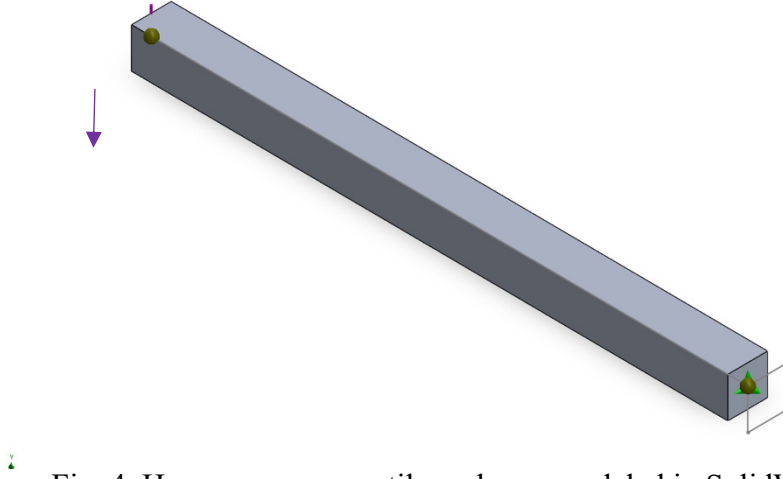


Fig. 4. Homogeneous, cantilever beam modeled in SolidWorks.

$$EI \frac{d^2w}{dx^2} = -M(x) = Px \quad (2)$$

$$\frac{d^2w}{dx^2} = \frac{P}{EI} x \quad (3)$$

Now, double integrating the above equation yields,

$$\frac{dw}{dx} = \frac{P}{EI} \int x dx \quad (4)$$

$$\frac{dw}{dx} = \frac{P}{2EI} x^2 + C_1 \quad (5)$$

$$w = \int \left(\frac{P}{2EI} x^2 + C_1 \right) dx \quad (6)$$

$$w = \frac{Px^3}{6EI} + C_1x + C_2 \quad (7)$$

Putting the boundary condition as $w = 0$ and $\frac{dw}{dx} = 0$ at $x = L$, the integral constants are determined as

$$C_1 = -\frac{PL^2}{2EI}, C_2 = \frac{PL^3}{3EI} \quad (8)$$

So, deflection at any point at distance x from the free end is given by,

$$w(x) = \frac{Px^3}{6EI} - \frac{PL^2}{2EI}x + \frac{PL^3}{3EI} \quad (9)$$

The deflection at the free end of the rectangular cantilever beam is

$$w(0) = \frac{PL^3}{3EI} \quad (10)$$

and the moment of inertia is

$$I = \frac{bh^3}{12} \quad (11)$$

It can be defined as: Again, for a homogeneous cross-section cantilever beam with constant material properties, the displacement value according to Timoshenko beam theory can be expressed as follows:

Let us assume that the clamped end is at $x = L$ and the free end is at $x = 0$. If a point load P is applied to the free end in the positive y direction, a free-body diagram of the beam gives us

$$-Px - M(x) = 0 \rightarrow M(x) = -Px \quad (12)$$

$$P + Q(x) = 0 \rightarrow Q(x) = -P \quad (13)$$

Therefore, from the expressions for the bending moment and shear force, we have

$$Px = EI \frac{d\varphi}{dx} \text{ and, } -P = kAG \left(-\varphi + \frac{dw}{dx} \right). \quad (14)$$

where k is the shear correction factor, G is the shear modulus, A is the cross-sectional area, and φ is the angle of rotation of the cross-section. Integration of the first equation, and application of the boundary condition $\varphi = 0$ at $x = L$, leads to

$$\varphi(x) = -\frac{P}{2EI} (L^2 - x^2). \quad (15)$$

The second equation can then be written as

$$\frac{dw}{dx} = -\frac{P}{kAG} - \frac{P}{2EI} (L^2 - x^2). \quad (16)$$

Integration and application of the boundary condition $w = 0$ at $x = L$ gives

$$w(x) = \frac{P(L-x)}{kAG} - \frac{Px}{2EI} \left(L^2 - \frac{x^2}{3} \right) + \frac{PL^3}{3EI} \quad (17)$$

The deflection at the free end of the cantilever beam is

$$w(0) = \frac{PL}{kAG} + \frac{PL^3}{3EI} \quad (18)$$

Since all these variables will change with the material we choose and the dimensions of the beam, we need to give the properties and dimensions of the material we choose:

Table 1. The values used in this study for an aluminum (5052-O) homogeneous cantilever beam

Variable	Symbol	Value	Unit
Singular Load	P	1000	N
Length	L	250,500,...,5000	cm
Height	h	50	cm
Width	b	50	cm
Cross-Section Area	A	bh	cm ²
Moment of Inertia	I	bh ³ /12	cm ⁴
Young's Modulus	E	7000000	N/cm ²
Poisson's Ratio	ν	0.33	-
Shear Correction Factor	k	5/6	-
Shear Modulus	G	$E/(2+2\nu)$	N/cm ²

As can be seen in Table 1, these values are repeated each time by increasing the length by 250 cm to provide different slenderness ratios.

3. Results and Discussion

In this section, the displacement behavior of homogeneous cross-section beams with variable slenderness ratios under load is examined within the framework of slenderness ratios. Results are given for the cases where one end of the beam is fixed and the other end is free. Firstly, a comparison was made with the SolidWorks simulation program to prove the validity and sensitivity of the solution methods used. The Solidworks simulation program separated this cantilever beam into a certain number of finite elements as seen in Fig. 5.

In Table 2, the maximum displacement values of homogeneous cantilever beams are compared with the SolidWorks simulation of Timoshenko and Bernoulli-Euler beam theories for various slenderness ratios. When the results are examined (examining the analysis result screen in Fig. 6. may also give an idea.), it can be said that the results obtained in this study are in excellent agreement with the other results.

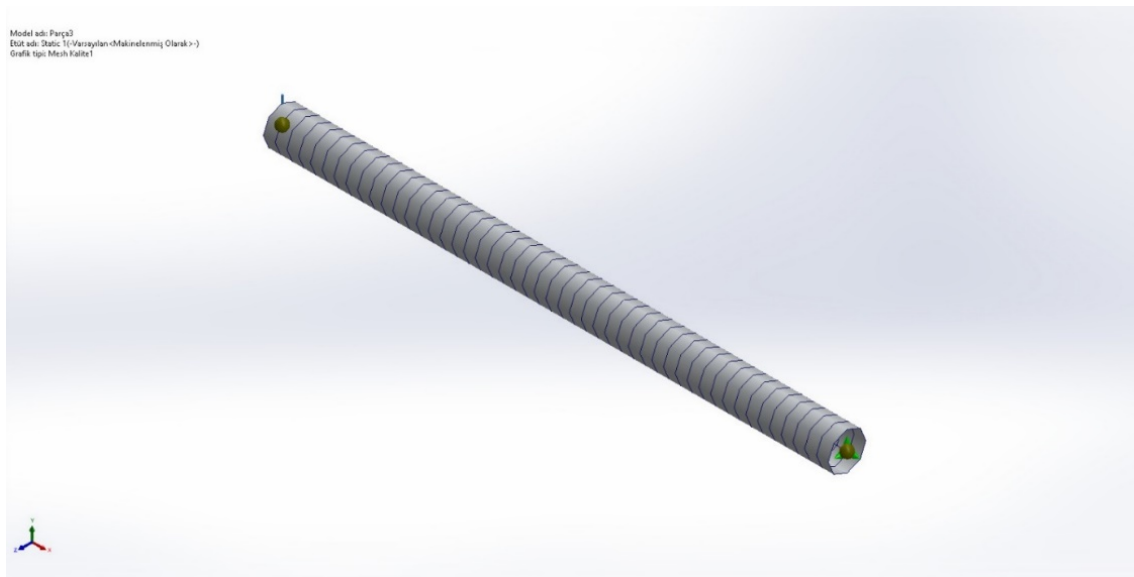


Fig. 5. Separation of the beam into finite elements.

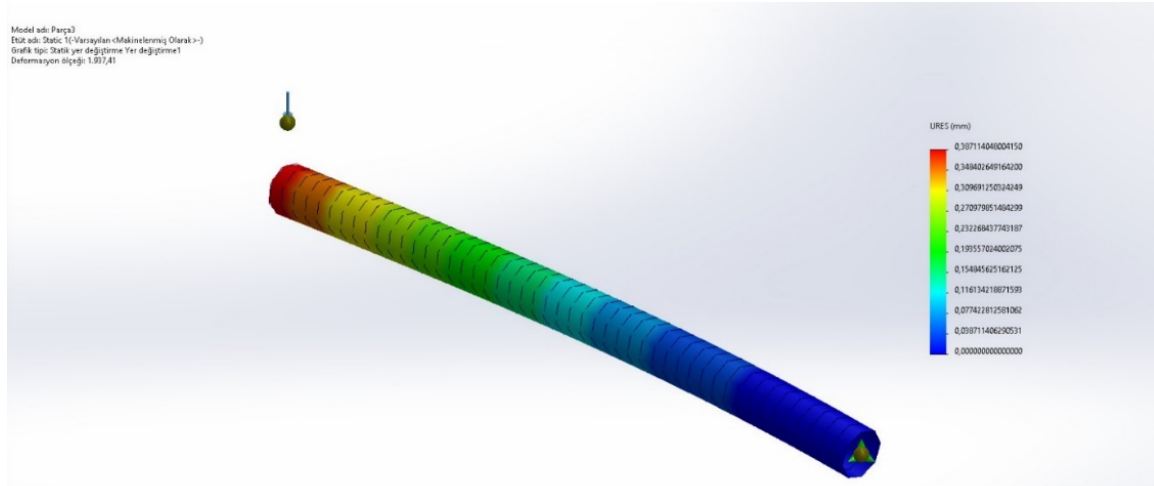


Fig. 6. Analysis result screen

Table 2. Comparison of beam theories with SolidWorks on the maximum displacements (*cm*) with respect to various slenderness ratios

Slenderness Ratio (L/h)	Bernoulli-Euler	Timoshenko	SolidWorks
5	0,001428571	0,001474171	0,001475231
10	0,011428571	0,011519771	0,011521892
15	0,038571429	0,038708229	0,038711405
20	0,091428571	0,091610971	0,091615212
30	0,308571429	0,308845029	0,308851331
40	0,731428571	0,731793371	0,731801891
50	1,428571429	1,429027429	1,429038048
60	2,468571429	2,469118629	2,469130993
70	3,920000000	3,920638400	3,920653152
80	5,851428571	5,852158171	5,852175236
90	8,331428571	8,332249371	8,332266808
100	11,428571430	11,42948343	11,42950439

Table 3. Comparison of % differences in maximum displacements with respect to various slenderness ratios

Slenderness Ratio (L/h)	Bernoulli-Euler – Timoshenko % Difference	Timoshenko – SolidWorks % Difference
5	3,093263044	1,234213101
10	0,791682375	0,523117832
15	0,353413228	0,465995258
20	0,199102790	0,399235343
30	0,088588119	0,297550460
40	0,049850137	0,243612856
50	0,031909814	0,266442410
60	0,022161754	0,181457275
70	0,016283062	0,145875785
80	0,012467195	0,138543153
90	0,009850881	0,127191497
100	0,007979363	0,108483805

Table 4. Number of Nodes - Number of Elements Comparison of SolidWorks Analyses

Slenderness Ratio (L/h)	Number of Nodes	Number of Elements
5	25	23
10	39	37
15	50	48
20	60	58
30	79	77
40	95	93
50	110	108
60	124	122
70	137	135
80	149	147
90	161	159
100	173	171

The % differences between the displacement values of a homogeneous cantilever beam for different slenderness ratios are tabulated in Table 3 and plotted in Fig. 7. It can be observed that the % difference of Bernoulli-Euler beam theory gradually decreases as the slenderness ratio value increases. Timoshenko beam theory, on the other hand, despite its low % difference, has a % difference value that decreases even more as the slenderness ratio increases.

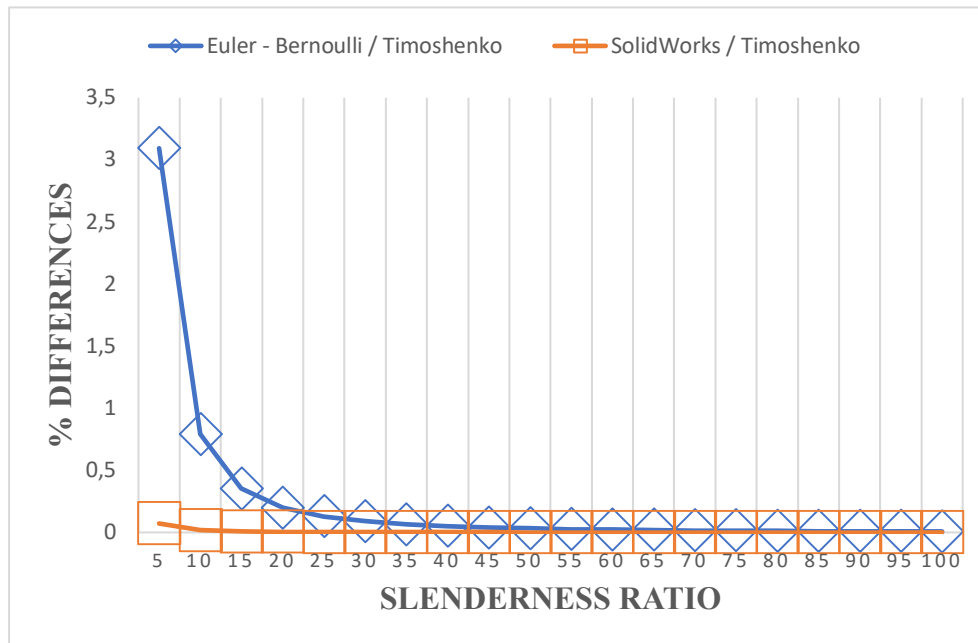


Fig. 7. Comparison of % differences

Fig. 8. and Table 4 show the Number of Nodes - Number of Elements. As can be seen here, the relationship between Number of Nodes - Number of Elements has a constant increase.

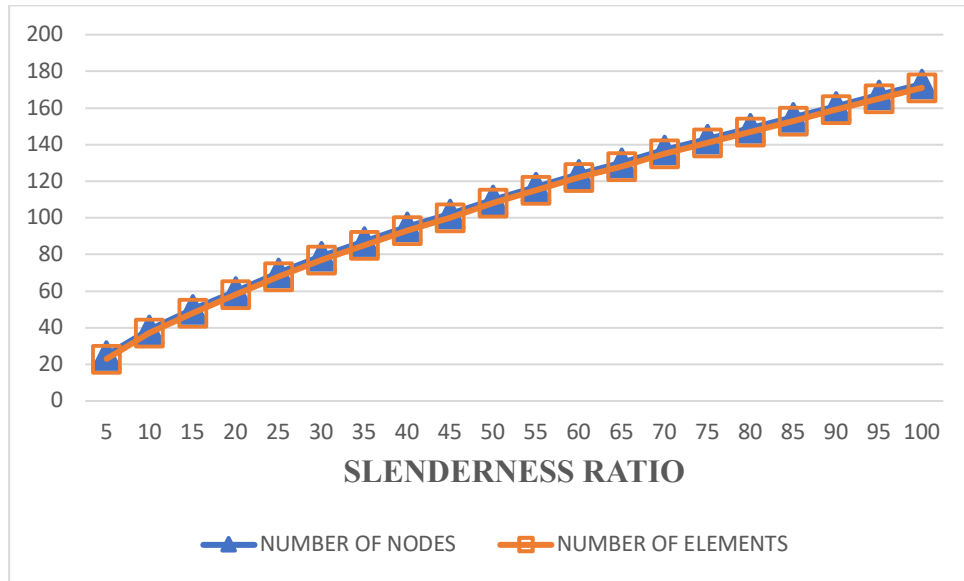


Fig. 8. Comparison of Number of Nodes - Number of Elements

4. Conclusions

In this study, the displacement behavior of cantilever beams with homogeneous cross-sections and various slenderness ratios subjected to point load was examined. The results obtained using Bernoulli-Euler and Timoshenko beam theories are compared with the results obtained from the simulation program SolidWorks. While it has been observed that the Timoshenko beam theory produces results very close to the simulation program values and the % difference decreases as the slenderness ratio increases, it has also been observed that the Bernoulli-Euler beam theory obtains results very close to reality as the slenderness ratio increases. With this inference, Timoshenko beam theory produces results very close to reality in beams with low slenderness ratio, while Bernoulli-Euler produces results very close to reality and very close to the results obtained from Timoshenko beam theory in beams with high slenderness ratio. In other words, it has been concluded that the effect of shear deformation and moment of inertia values, which are effective in Timoshenko beam theory, on the displacement value decreases as the slenderness ratio increases. Moreover, if we compare all the data we obtained, we see that SolidWorks gives us results very close to the theoretical solution. For this reason, when it is not possible to make a theoretical solution, when larger and more complex problems need to be solved in a shorter time, very good results can be obtained with SolidWorks. Since SolidWorks makes a solution based on FEM, no matter how large or complex the systems are, good results can be obtained as long as proper modeling is done. In addition, when the results obtained in this article are interpreted properly, correct inferences can be made at the nanomechanics and can be used to give ideas in studies to be carried out at the nanomechanics.

Author Contributions

Bekir Akgöz: Designed and directed the paper, Verified the theories and methods, Conceived and designed the analysis, Contributed data and analysis tools, Prepared the paper for publication.

Alper Oğulcan Söylemez: Conducted a literature review, Collected the data, Performed the analysis, Wrote the paper, Prepared the paper for publication.

References

- [1] Alibakhshi, A., Rahmanian, S., Dastjerdi, S., Malikan, M., Karami, B., Akgöz, B., Civalek, Ö., Hyperelastic Microcantilever AFM: Efficient Detection Mechanism Based on Principal Parametric Resonance, *Nanomaterials*, 12(15), 2022.
- [2] Euler, L., Methodus Inveniendi Lineas Curvas Sive Solutio Problematis Isoperimetrici Latissimo Sensu Accepti, Marcus-Michael Bousquet, 1744.
- [3] Timoshenko, S.P., Gere, J.M., Theory of Elastic Stability, McGraw-Hill Book Co. Inc., 2nd Edition, 1961.
- [4] Timoshenko, S.P., Gere J.M., Mechanics of Materials, Boston: PWS Pub Co., 4th Edition, 1997.
- [5] Wang, C.M., Wang, C.Y., Reddy, J.N., Exact Solutions for Buckling of Structural Members, CRC Press LLC, 2005.
- [6] Zienkiewicz, O.C., Taylor, R.L., The Finite Element Method for Solid and Structural Mechanics, Butterworth-Heinemann, 6th edition, 2005.
- [7] Bazant Z.P., Cedolin L., Stability of Structures: Elastic, Inelastic, Fracture and Damage Theories, World Scientific Publishing Co. Pte. Ltd., 2010.
- [8] Ghali. A., Neville, A.M., Structural Analysis: A Unified Classical and Matrix Approach, CRC Press LLC, 7th edition, 2009.
- [9] Cook, R.D., Malkus, D.S., Plesha, M.E., Concepts and Applications of Finite Element Analysis, John Wiley & Sons Inc, 3rd edition, 2002.
- [10] Akgöz, B., Civalek, Ö., Investigation of size effects on static response of single-walled carbon nanotubes based on strain gradient elasticity. *International Journal of Computational Methods*, 9(02), 1240032, 2012.
- [11] Akgöz, B., Mercan, K., Demir, Ç., Civalek, Ö., Static analysis of beams on elastic foundation by the method of discrete singular convolution. *International Journal of Engineering and Applied Sciences*, 8(3), 67-73, 2016.
- [12] Van Vinh, P., Van Chinh, N., & Tounsi, A., Static bending and buckling analysis of bi-directional functionally graded porous plates using an improved first-order shear deformation theory and FEM. *European Journal of Mechanics-A/Solids*, 96, 104743, 2022.
- [13] Yaylacı, M., Yaylacı, E. U., Özdemir, M. E., Öztürk, Ş., Sesli, H., Vibration and buckling analyses of FGM beam with edge crack: Finite element and multilayer perceptron methods. *Steel and Composite Structures*, 46(4), 565-575, 2023.
- [14] Azizi, A., Dourali, L., Zareie, S., Rad, F. P., Mathematical Modeling of Deflection of a Beam: A Finite Element Approach. *2009 Second International Conference on Environmental and Computer Science*, Dubai, UAE, 2009.
- [15] Oladejo, K. A., Abu, R., Bamiro, O. A., Model for deflection analysis in Cantilever Beam. *European Journal of Engineering and Technology Research*, 3(12), 60-66, 2018.
- [16] Chaphalkar, S.P., Khetre, S.N., Meshram, A.M., Modal analysis of cantilever beam Structure Using Finite Element analysis and Experimental Analysis. *American Journal of Engineering Research*, 4(10), 178-185, 2015.

- [17] Hodzic, D., Bending Analysis of Cantilever Beam in Finite Element Method. *Annals of the Faculty of Engineering Hunedoara-International Journal of Engineering*, 19(4), 23-26, 2021.
- [18] Raj, R., Sinha, P. K., Prakash, E. V., Modelling, Simulation and Analysis of Cantilever Beam of Different Material by Finite Element Method, ANSYS & MATLAB. *International Journal of Engineering Research and General Science*, 3(3), 89-100, 2015.
- [19] Quang, K. L. T., My, D. D. T., & Van, B. T., Structural analysis of continuous beam using finite element method and ANSYS. *Journal of Materials & Construction*, 11(02), 60-65, 2021.
- [20] Ho, M., Lee, P., Ye, C., Lin, C., Huang, C., Experiment and finite element analysis study on the deflection of aluminum extruded 6063-T5 hollow structural beam, *IOP Conference Series: Materials Science and Engineering*, 711(1), 012075, 2020.
- [21] Samal, A. K., Rao, T. E., Analysis of Stress and Deflection of Cantilever Beam and its Validation Using ANSYS. *Ashis Kumar Samal Int. Journal of Engineering Research and Applications*, 6(1), 119-126, 2016.
- [22] Balart Gimeno, R. A., Quiles Carrillo, L. J., Montañés Muñoz, N., A comparison between the analytical solution of a single cantilever beam fixed at one end and the use of the finite elements method (FEM) with SolidWorks. <http://hdl.handle.net/10251/103904>, 2018.
- [23] Balart Gimeno, R. A., Quiles Carrillo, L. J., Montañés Muñoz, N., Interpretation of the results obtained by Finite Element Analysis (FEA) in SolidWorks. <http://hdl.handle.net/10251/104404>, 2018.
- [24] Balart Gimeno, R. A., Quiles Carrillo, L. J., Montañés Muñoz, N., Creating a CAD model of a single beam for engineering analysis with SolidWorks. <http://hdl.handle.net/10251/103904>, 2018.
- [25] Onimowo, E., Onimowo D., Numerical Analysis of a Cantilever Beam and Validation Using Theoretical Methods with Application to Unit Delivery, *Authorea Preprints*, 2020.
- [26] Ya, T. T., Alebrahim, R., Fitri, N., Alebrahim, M., Analysis of Cantilever Beam Deflection under Uniformly Distributed Load using Artificial Neural Networks. *MATEC Web of Conferences*, 255, 06004, 2019.
- [27] Talebi Rostami, H., Fallah Najafabadi, M., Ganji, D. D., Analysis of Timoshenko beam with Koch snowflake cross-section and variable properties in different boundary conditions using finite element method. *Advances in Mechanical Engineering*, 13(11), 2021.
- [28] Gao, J., Deflection Study on Beams with COMSOL Finite Element Analysis, Degree Thesis, Arcada University of Applied Sciences, 2020.
- [29] Onwubolu, G. C., Computer-Aided Engineering Design with SolidWorks, Imperial College Press, 1st Edition, 2011.
- [30] Reddy J.N., On Locking-Free Shear Deformable Beam Finite Elements. *Computer Methods in Applied Mechanics and Engineering*, 149(1-4), 113-132, 1997.
- [31] Timoshenko, S.P., *History of strength of materials*, McGraw-Hill Book Co. Inc., 1st Edition, 1953.

Effect of Evaporation and Condensation Temperature on Performance of Organic Rankine System Using R134a, R417A, R422D, R245fa

Erkan Dikmen ^{a*}, Arzu Şencan Şahin ^b

Mechanical Engineering, Faculty of Technology, Isparta University of Applied Sciences, Isparta, Türkiye

✉ : erkandikmen@isparta.edu.tr^{a*}, arzusencan@isparta.edu.tr^b,  : 0000-0002-6804-8612^{a*}, 0000-0001-8519-4788^b

Received: 11.08.2024, Revised: 18.11.2024, Accepted: 20.11.2024

Abstract

Organic Rankine Cycles (ORCs) are identified as one of the most promising technologies for generating electricity from low-grade heat sources. Unlike conventional Rankine cycles, ORCs operate at lower temperatures and pressures. This allows them to utilize organic fluids or refrigerants as the working fluid instead of water, which is better suited for high-pressure and high-temperature applications. The performance and design of an ORC system are heavily dependent on the chosen working fluid. Therefore, selecting the right working fluid is crucial for a specific application, such as solar thermal, geothermal, or waste heat recovery. This study analyzed the performance of ORCs using four different working fluids: R-134a, R-245fa, R417A, and R422D. The researchers investigated how variations in condensation and evaporation temperatures affect thermal efficiency, mass flow rate, pump power, and turbine pressure ratio. The Engineering Equation Solver (EES) program was used for analyses. The results demonstrated that condensation and evaporation temperatures significantly influence system performance. The study found that ORC systems using R417A and R422D exhibited higher efficiencies compared to the other working fluids analyzed. Additionally, these fluids required lower mass flow rates per unit of power generation compared to the other fluids.

Keywords: Organic Rankine Systems, Working fluids, Performance.

1. Introduction

As human society advances, we confront a growing energy crisis and environmental challenges due to our energy consumption. Fortunately, a solution exists: utilizing medium-low grade thermal energy. This includes recovering waste heat and employing renewable and sustainable energy sources. The Organic Rankine Cycle (ORC) has emerged as a popular and promising technology for harnessing this abundant, yet often underutilized, energy source [1-4].

Several review papers on Organic Rankine Cycles (ORCs) have emerged in recent years. Park et al. focused on performance of experimental ORC, analyzing and reporting key data on prototypes, developed systems, and current trends [5]. Focusing on waste heat recovery, Tartière and Astolfi analyzed the evolution of the ORC market and its diverse applications. Additionally, they explored the technology's future prospects and potential for market growth [6]. Pethurajan et al. conducted a bibliographic review on selecting turbines for ORCs and their applications in topping or bottoming cycles [7]. Additionally, Haghighi et al. and Ahmadi et al. presented bibliographic reviews on geothermal ORCs. Both studies focused on analyzing basic ORCs, ORCs with recuperators, and regenerative ORCs for electricity generation [8,9]. Haghighi et al. primarily concentrated on modeling and optimizing ORCs using various working fluids, reporting energy and exergy efficiency values [9]. Ahmadi et al. carried out a comprehensive analysis focusing on economic factors like levelized cost of electricity and electricity production cost. Their study also included a comparative analysis of these factors with conventional power generation systems, expanding their findings [8]. Finally, Wieland et al. discussed recent advancements and future market perspectives for ORCs. While these



reviews cover diverse topics, they primarily center on basic ORC systems. Several studies have focused on identifying optimal working fluids for ORCs from a thermodynamic perspective [10]. Zhang et al. investigated 57 fluids by analyzing their saturated vapor curves. They categorized the fluids into wet, dry, and isentropic classifications. Their research showed that the area of the triangle formed by the critical point and the saturated conditions at the turning point has a significant impact on performance of system. Notably, R123 fluids exhibited the best performance among the studied fluids [11]. A new method for finding the best working fluids for low temperature ORC applications is described by Györke et al. and Imre et al. The method uses a relationship between a specific property of the working fluid in its saturated vapour state to identify optimal fluids for low-temperature ORCs [12,13]. Blondel et al. investigated zeotropic mixtures as potential working fluids of ORCs. They suggested new, semi-empirical heat transfer correlations for both evaporator and condenser processes. Additionally, they evaluated how heat source characteristics (low and high temperatures) affect cycle performance. Interestingly, their findings suggest that zeotropic mixtures with low temperature glide values may not offer significant performance advantages compared to pure fluids [14]. Yang et al. investigated the connection between critical temperatures and boiling temperatures for a wide range of over 250 potential working fluids in ORCs. The relationship between critical temperature and maximum net power remained significant even with variations in reduced boiling temperature, specifically within the temperature range of 150 °C to 200 °C [15]. A method to directly link specific properties of working fluids to the overall performance of an ORC system by Fan et al. was developed [16]. Zhang and Li investigated the behavior of "super-dry" working fluids in regenerative ORC systems designed for medium and low temperature heat sources [17]. Bahrami et al. reviewed low GWP working fluids for ORC applications. Their study explored methodologies for selecting working fluids and considered alternative options such as hydrocarbons, hydrofluorochemicals, and even mixtures [18].

In this study, the effect of condensation and evaporation temperatures on performance of the system operating with 4 different working fluids accepted to be used in ORC systems in the literature was investigated. There are many studies on ORC systems. In this study, unlike the literature, comparative thermodynamic analysis of R134a, R417A, R422D (isentropic) and R245fa (dry) working fluids were performed. Thermodynamic analysis was performed using the EES program.

2. ORC System Description

A basic ORC system comprises four fundamental components: a condenser, an evaporator, an expander, and a pump. Figure 1 shows the basic configuration of an ORC system. As shown, the liquid is pumped to a higher-pressure state (2) from a saturated condition (1) by the pump prior to entering the evaporator. In the evaporator, heat is introduced, resulting in the evaporation of the liquid (3). Subsequently, the working fluid expands in the expander (4), thereby generating power as its pressure decreases. Subsequently, the fluid enters the condenser, where it undergoes a phase transition back into a liquid state (1), thereby completing the cycle. This ORC system is sometimes called a single-stage ORC due to its use as the single evaporator [19].

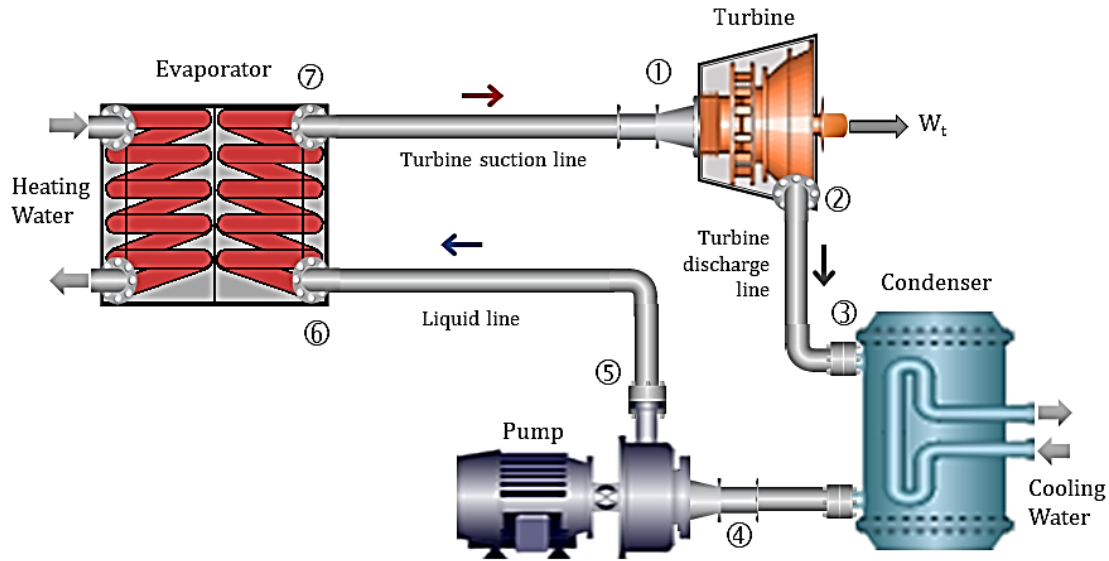


Fig.1. Schematic diagram of basic an ORC system

3. Working Fluid Selection

The selection of a working fluid for an ORC system is crucial. The type of fluid directly affects the cycle's operating parameters and overall efficiency. The shape of a working fluid's saturation vapor curve is a critical property for ORC systems. This characteristic significantly impacts the fluid's suitability, the cycle's overall efficiency, and even the configuration of equipment needed within the power generation system [20,21]. The temperature-entropy ($T-s$) diagram typically shows three categories of vapor saturation curves (Fig. 2). These categories are:

- Dry fluid: The curve has positive slopes.
- Wet fluid: The curve has negative slopes.
- Isentropic fluid: The curve has slopes approaching positive infinity.

Because the saturation vapor curve for a wet fluid has a negative slope, the turbine's outlet stream typically contains a significant amount of saturated liquid. The presence of liquid inside the turbine can damage the turbine blades and also reduce the turbine isentropic efficiency. The amount of vapor remaining in the turbine outlet (dryness fraction) needs to be above 85%. To achieve this dryness requirement with a wet working fluid entering the turbine, superheating is necessary. However, superheating comes with drawbacks. Heat transfer in the vapor phase has a lower coefficient, which significantly increases the required heat transfer area and consequently raises the cost of the superheater. Additionally, superheaters can introduce other operational challenges. Fortunately, 'isentropic' and 'dry' fluids eliminate the need for superheating altogether. This avoids the potential damage caused by liquid droplets impacting the turbine blades. Since superheating is not required, there's no need for the additional equipment associated with it. Therefore, 'dry' or 'isentropic' working fluids are better suited for ORC systems [21]. Therefore, dry (R245fa) and isentropic (R134a, R417A, and R422D) working fluids are selected in this study. Table 1 provides information on working fluid properties and selection criteria.

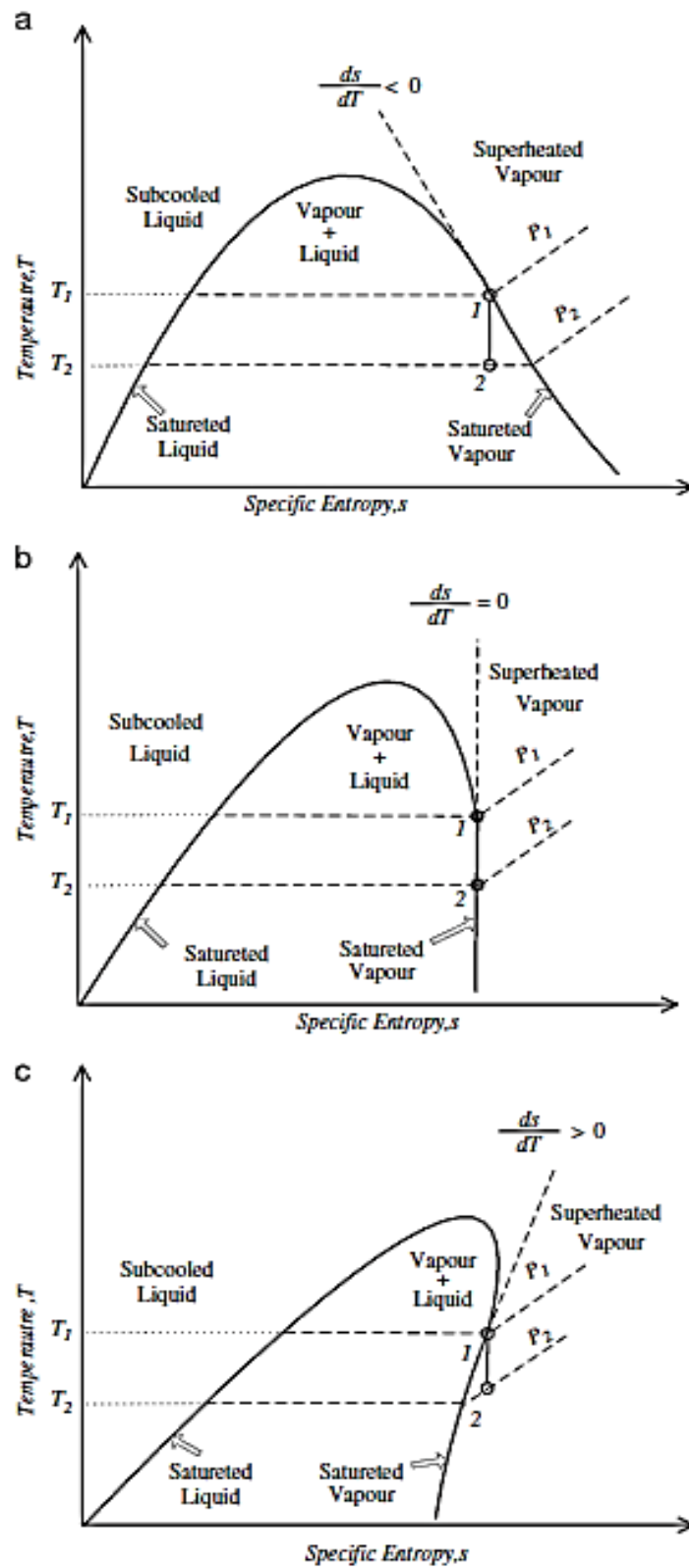


Fig. 2. Diagrams $T-s$ for different fluids (a) wet,(b) isentropic and (c) dry [20].

Table 1. Working fluid properties and selection criteria [22].

Refr.	Critical temp. (°C)	Critical pressure (MPa)	Normal boiling point (°C)	Ozone depleting potential (ODP)	Global warming potential (GWP)	Safety level (Ashrae)	Heat source temp. (°C)	Remarks
R134a	101.06	4.0592	-26.3	0.06	1430	A1	80.848	Due to its negative boiling point, R134a is an appropriate isentropic working fluid for small systems.
R417A	87.04	4.036	-	0.0	2346	A1	69.632	It is accepted that R417A is a zeotropic fluid
R422D	79.56	3.903	-	0.0	2729	A1	63.648	It is accepted that R422A is a zeotropic fluid
R245fa	154.05	3.640	15.0	0.0	1030	B1	123.24	R245fa is a dry working fluid. With due consideration of the relevant environmental parameters, it is therefore deemed to be acceptable.

4. Research Method

Thermodynamic analysis of the ORC system is based on applying the mass and energy equations for each process, as shown in Figure 1. The thermodynamic analysis was carried out using the Engineering Equation Solver (EES). The ORC system consists of four main components: condenser, pump, evaporator, and turbine, which are steady-state flow devices. Therefore, the four processes that make up the ORC can be treated as a steady flow process, and these processes can be analyzed using the relevant thermodynamic equilibrium and equations expressed as [23,24]:

$$(Q_{in} - Q_{out}) + (W_p - W_t) = m_r(h_{out} - h_{in}) \quad (1)$$

The processes of evaporator and condenser do not any input of work and the pump and turbine can be regarded as isentropic. Therefore, the relationship between the input and output energies for each of these components can be expressed as follows:

a) The power required for the pumping of the condensed liquid working fluid to the intake side of the boiler is calculated using the following equation:

$$W_p = \frac{m_r(h_5 - h_4)}{\eta_p} \quad (2)$$

b) In a boiler, heat is introduced to the liquid working fluid, resulting in a phase change to a gaseous state. Using the following formula, the boiler's necessary calorific value is determined:

$$Q_{in} = m_r(h_7 - h_6) \quad (3)$$

c) The turbine power is produced by the expansion of the working fluid from a high-pressure state to a condensing state in gaseous form; the output power is determined by the following equation:

$$W_t = m_r \eta_t (h_1 - h_2) \quad (4)$$

d) For the condenser, a specific quantity of heat is released into the environmental air. This heat released can be calculated using the following equation:

$$Q_{out} = m_r(h_3 - h_4) \quad (5)$$

The following formula is used to calculate thermal efficiency, which is usually used to assess the effectiveness of ORC systems:

$$\eta_{th} = \frac{W_{out}}{Q_{in}} = \frac{(W_t - W_p)}{Q_{in}} \quad (6)$$

The parameters and assumptions presented in Table 2 have been selected on the basis of the operational ranges of ORC systems that have been employed as small-scale power plants.

Table 2. Parameters and assumptions used in research

<i>Parameter</i>	<i>Unit</i>	<i>Value</i>
<i>Turbine output power</i>	kW	60
<i>Turbine inlet temperature</i>	°C	77; 75; 72; 69; 66; 63
<i>Condensing temperature</i>	°C	28; 31; 34; 37; 40; 43
<i>Turbine isentropic efficiency</i>		0.82
<i>Pump isentropic efficiency</i>		0.73

5. Result and Discussion

The mass flow rate, pumping power consumption, turbine pressure ratio and thermal efficiency of the ORCs for four fluids have been calculated for a range of evaporator temperature, as seen in the Figures 3-6. Fig. 3 gives the effect of evaporation temperature on the mass flow rate of the working fluids in the ORC system with the condensation temperature held constant at 34 °C. It can be seen that increasing the evaporation temperature results in a decrease in the mass flow rate of the working fluids in the system. The mass flow rate of R422D and R417A are lower than R134a and R245fa.

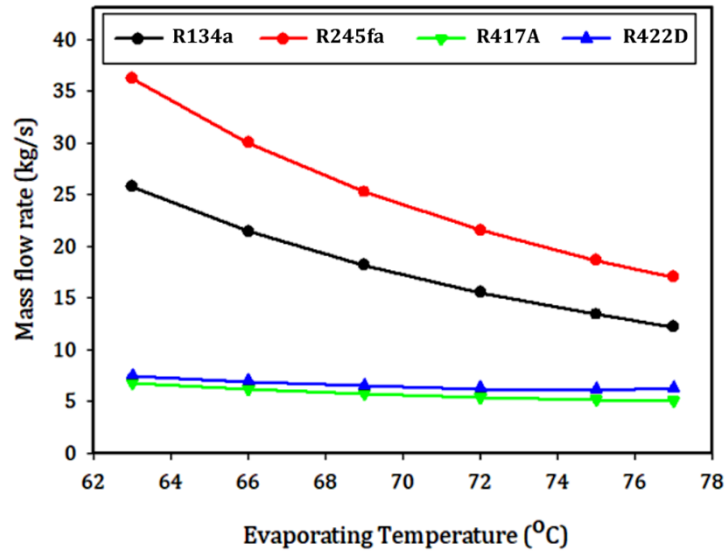


Fig. 3. Effect of evaporation temperature on mass flow rate of working fluid at $T_{\text{condensing}}=34^{\circ}\text{C}$

Fig. 4 presents the effect of evaporation temperature on the pumping power consumption of the working fluids in the ORC system with the condensation temperature held constant at 34°C . The pumping power with increasing the evaporation temperature in the system decrease for R134a and R245fa. However, in the ORC system operating with R422D and R417A fluids, it was observed that the pumping power increased with increasing evaporator temperature. The pumping power to circulate R134a is much greater than the other three working fluids.

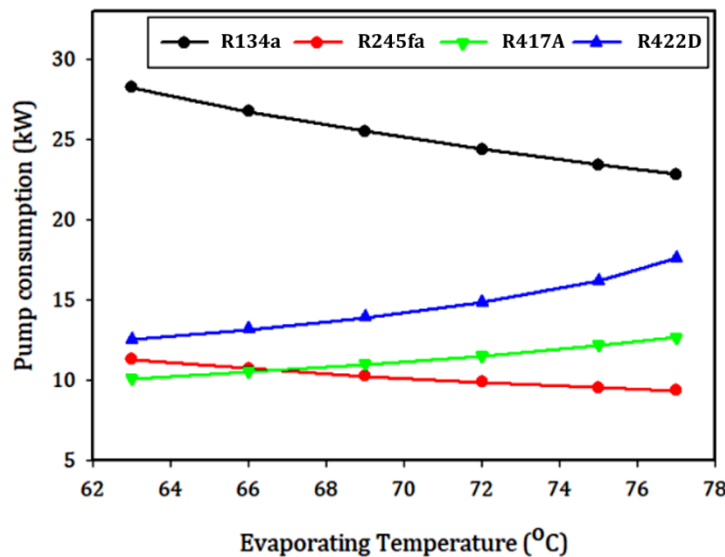


Fig. 4 Effect of evaporating temperature on pumping power consumption at $T_{\text{condensing}}=34^{\circ}\text{C}$

Fig. 5 shows the turbine pressure ratio against the evaporating temperature for four different working fluids. The turbine pressure ratio of all four refrigerants increases as the evaporating temperature increases. The ORC system using R245fa has a higher turbine pressure ratio of 40% compared to the other three working fluids.

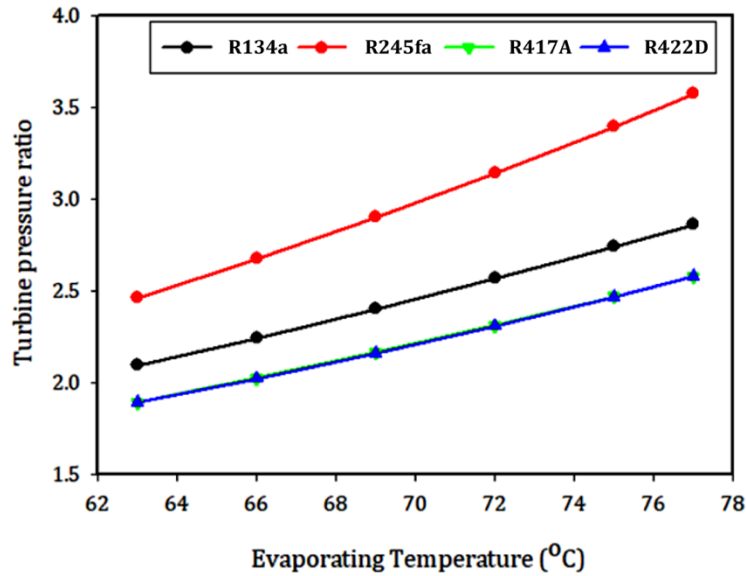


Fig.5 Effect of evaporation temperature on pressure ratio in turbine at $T_{\text{condensing}} = 34^{\circ}\text{C}$

Fig. 6 shows that the thermal efficiency of working fluids decreases as the evaporating temperature increases. R422D and R417A is the most efficient fluids at all evaporating temperatures, followed by R134a and R245fa.

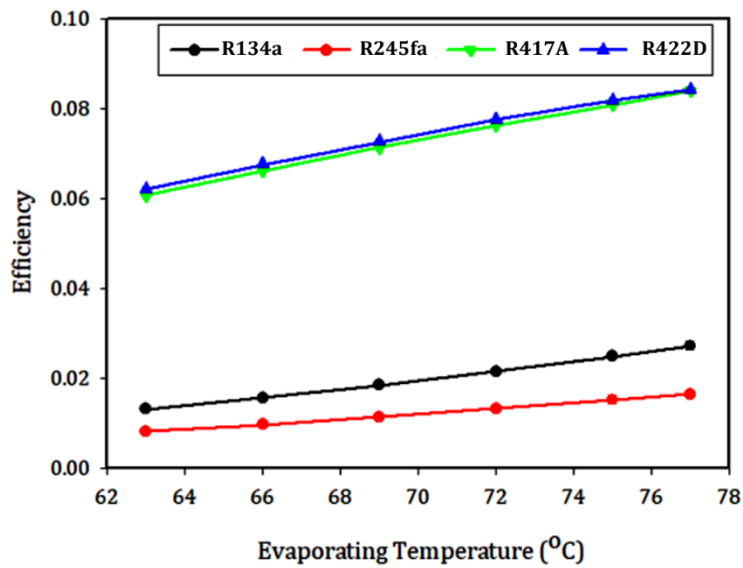


Fig. 6. Effect of evaporation temperature on system thermal efficiency at $T_{\text{condensing}} = 34^{\circ}\text{C}$

Fig. 7 gives the mass flow rate of four different refrigerants (R134a, R245fa, R417A, and R422D) as a function of condensing temperature at 72°C evaporation temperature. The mass flow rate increases as the condensing temperature increases for all four refrigerants. R245fa has the highest mass flow rate, followed by R134a, R422D, and R417A.

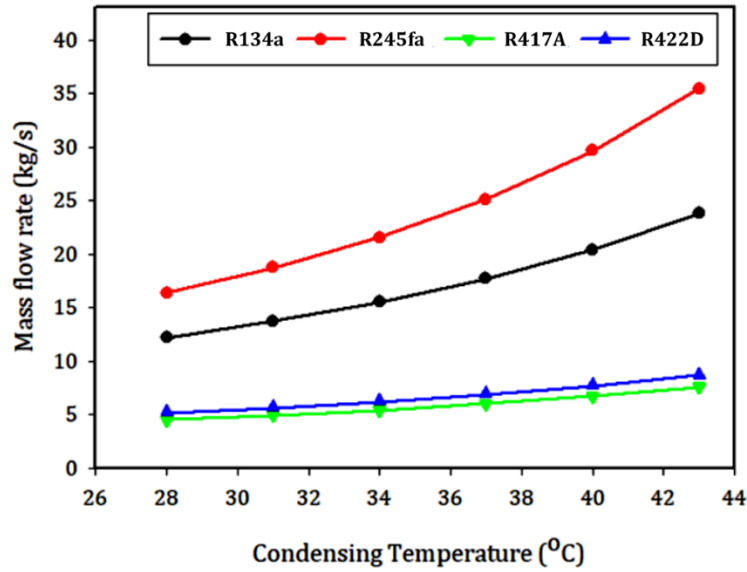


Fig. 7. Effect of the condensation temperature on the mass flow rate of the working fluid at $T_{\text{evaporating}}=72^{\circ}\text{C}$

As can be seen Fig. 8, as the condensation temperature increases, the pumping power required will also increase. Although the mass flow rate of R245fa is higher than that of R134a, the pumping power used to circulate R245fa in the ORC system is % 53 lower than that of R134a. The pumping power to R134a is much greater than the other three working fluids.

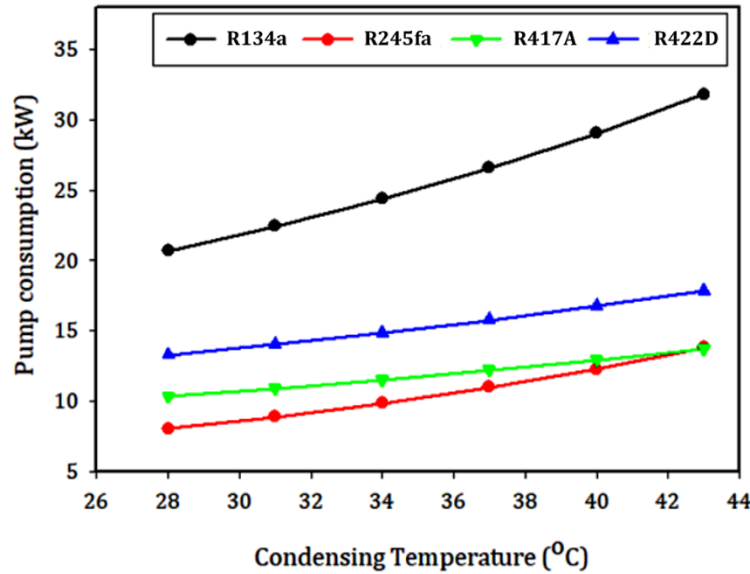


Fig. 8. Effect of condensing temperature on pumping power consumption at $T_{\text{evaporating}}=72^{\circ}\text{C}$

Fig. 9 shows that the turbine pressure ratio decreases as the condenser temperature increases. This is because the turbine pressure ratio is a measure of the turbine efficiency, and the efficiency of the turbine decreases as the condenser temperature increases. The ORC system using R245fa has a higher turbine pressure ratio of compared to the other three working fluids.

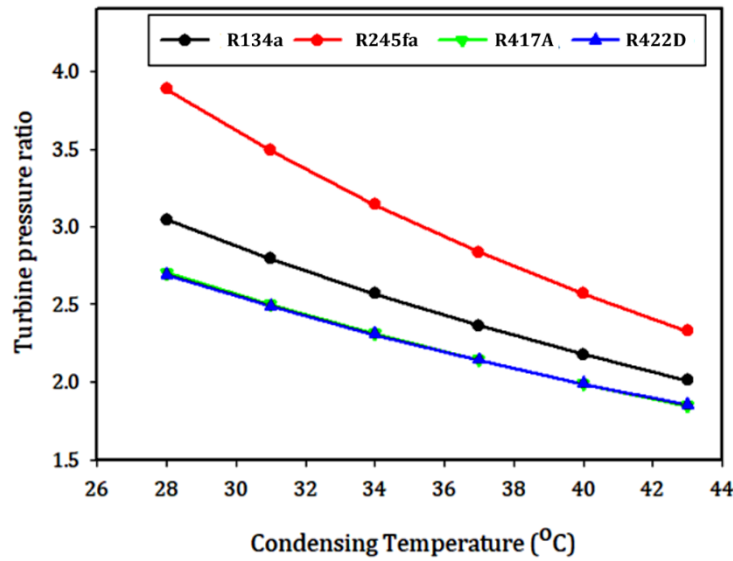


Fig. 9. Effect of condensation temperature on pressure ratio in turbine at $T_{\text{evaporating}}=72^{\circ}\text{C}$

Fig. 10 presents the relationship between the condensing temperature and the efficiency of four different refrigerants. The efficiency of all four fluids decreases as the condensing temperature increases. However, the thermal efficiency varies depending on the working fluid. R422D and R417A have the highest thermal efficiency, followed by R134a and R245fa.

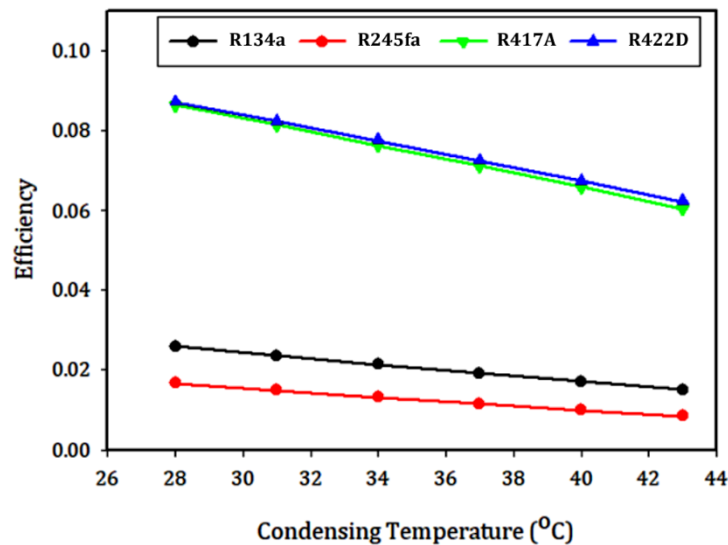


Fig. 10. Effect of condensation temperature on system thermal efficiency at $T_{\text{evaporating}}=72^{\circ}\text{C}$

6. Conclusions

This study examines the possible future use of isentropic (R134a, R422D and R417A) and dry (R245fa) acceptable working fluids in ORC systems. The study found that ORC systems using R417A and R422D exhibited higher efficiencies compared to the other working fluids analyzed. Since evaluating the optimal performance for each working fluid individually can be challenging, a common approach involves simulating the cycle using a thermodynamic model. This allows for a direct comparison of four working fluids against R422D and R417A. The study revealed that thermal efficiency rises with increasing evaporator temperature but falls as condenser temperature increases. Notably, this research identified R422D and R417A as

working fluids that deliver significantly improved efficiencies across a range of operating conditions compared to other organic Rankine cycle (ORC) fluids.

Author Contributions

Erkan Dikmen: Writing-original draft, Investigation, Conceptualization, Visualization, Analysis.

Arzu Şencan Şahin: Investigation, Supervision, Methodology, Conceptualization Writing-Review& editing.

References

- [1] Zhi, L. H., Hu, P., Chen, L. X., Zhao, G., Thermodynamic analysis of a novel transcritical-subcritical parallel organic Rankine cycle system for engine waste heat recovery. *Energy Conversion and Management*, 197, 111855, 2019.
- [2] Moreira, L. F., Arrieta, F. R. P., Thermal and economic assessment of organic Rankine cycles for waste heat recovery in cement plants. *Renewable and Sustainable Energy Reviews*, 114, 109315, 2019.
- [3] Hoang, A. T., Waste heat recovery from diesel engines based on Organic Rankine Cycle. *Applied Energy*, 231, 138–166, 2018.
- [4] Zhang, X., Zhang, Y., Wang, J., New classification of dry and isentropic working fluids and a method used to determine their optimal or worst condensation temperature used in Organic Rankine Cycle. *Energy*, 201, 117722, 2020.
- [5] Park, B.S., Usman, M., Imran, M., Pesyridis, A. Review of Organic Rankine Cycle experimental data trends. *Energy Conversion and Management*, 173, 679–691, 2018.
- [6] Tartière, T., Astolfi, M. A., World Overview of the Organic Rankine Cycle Market. *Energy Procedia*, 129, 2–9, 2017.
- [7] Pethurajan, V., Sivan, S., Joy, G. C., Issues, comparisons, turbine selections and applications – An overview in organic Rankine cycle. *Energy Conversion and Management*, 166, 474–488, 2018.
- [8] Ahmadi, A., El Haj Assad, M., Jamali, D. H., Kumar, R., Li, Z. X., Salameh, T., et al., Applications of geothermal organic Rankine Cycle for electricity production. *Journal of Cleaner Production*, 274, 122950, 2020.
- [9] Asadi, M., Khoshkhoo, R. H., Effects of Chevron Angle on Thermal Performance of Corrugated Plate Heat Exchanger. *International Journal of Engineering Practical Research*, 3(1), 8, 2014.
- [10] Wieland, C., Schiffelechner, C., Dawo, F., Astolfi, M., The organic Rankine cycle power systems market: Recent developments and future perspectives. *Applied Thermal Engineering*, 224, 119980, 2023.
- [11] Zhang, X., Zhang, C., He, M., Wang, J., Selection and Evaluation of Dry and Isentropic Organic Working Fluids Used in Organic Rankine Cycle Based on the Turning Point on Their Saturated Vapor Curves. *Journal of Thermal Science*, 28(4), 643–658, 2019.
- [12] Györke, G., Groniewsky, A., Imre, A.R., A simple method of finding new dry and isentropic working fluids for organic Rankine cycle. *Energies*, 12(3), 1–11, 2019.
- [13] Imre, A.R., Kustán, R., Groniewsky, A., Thermodynamic selection of the optimal working fluid for organic Rankine cycles. *Energies*, 12(10), 1–15, 2019.

- [14] Blondel, Q., Tauveron, N., Lhermet, G., Caney, N., Zeotropic mixtures study in plate heat exchangers and ORC systems. *Applied Thermal Engineering*, 219, 119418, 2023.
- [15] Yang, L., Gong, M., Guo, H., Dong, X., Shen, J., Wu, J., Effects of critical and boiling temperatures on system performance and fluid selection indicator for low temperature organic Rankine cycles. *Energy*, 109, 830–844, 2016.
- [16] Fan, W., Han, Z., Li, P., Jia, Y., Analysis of the thermodynamic performance of the organic Rankine cycle (ORC) based on the characteristic parameters of the working fluid and criterion for working fluid selection. *Energy Conversion and Management*, 211, 112746, 2020.
- [17] Zhang, X., Li, Y., An examination of super dry working fluids used in regenerative organic Rankine cycles. *Energy*. 263, 125931, 2023.
- [18] Bahrami, M., Pourfayaz, F., Kasaeian, A., Low global warming potential (GWP) working fluids (WFs) for Organic Rankine Cycle (ORC) applications. *Energy Reports*, 8, 2976–2988, 2022.
- [19] Jiménez-García, J. C., Ruiz, A., Pacheco-Reyes, A., Rivera, W. A. Comprehensive Review of Organic Rankine Cycles. *Processes*, 11(7), 1982, 2023.
- [20] Bao, J., Zhao, L., A review of working fluid and expander selections for organic Rankine cycle. *Renewable and Sustainable Energy Reviews*, 24, 325–342, 2013.
- [21] Liu, B. T., Chien, K. H. and Wang, C. C., Effect of working fluids on organic Rankine cycle for waste heat recovery. *Energy*, 29(8), 1207–1217, 2004.
- [22] Malwe, P., Gawali, B., Shaikh, J., Deshpande, M., Dhalait, R., Kulkarni, S., et al., Exergy assessment of an Organic Rankine Cycle for waste heat recovery from a refrigeration system: a review. *Chemical Engineering Communication*, 210(5), 837–865, 2023.
- [23] Cengel, Y. A., Boles, M. A., Thermodynamics: an engineering approach. McGraw-hill, 8nd Edition, 2015
- [24] Kong, R., Deethayat, T., Asanakham, A., Vorayos, N., Kiatsiriroat, T., Thermodynamic performance analysis of a R245fa organic Rankine cycle (ORC) with different kinds of heat sources at evaporator. *Case Studies in Thermal Engineering*, 13, 100385, 2019.